The Astrophysical Journal, 804:98 (22pp), 2015 May 10 doi:10.1088/0004-637X/804/2/98


# THE DEUTERIUM FRACTIONATION TIMESCALE IN DENSE CLOUD CORES: A PARAMETER SPACE EXPLORATION

Shuo Kong[1], Paola Caselli[2,3], Jonathan C. Tan[1,4], Valentine Wakelam[5,6], and Olli Sipilä[2]
[1] Dept. of Astronomy, University of Florida, Gainesville, FL 32611, USA; skong@astro.ufl.edu
[2] Max-Planck-Institute for Extraterrestrial Physics (MPE), Giessenbachstr. 1, D-85748 Garching, Germany; caselli@mpe.mpg.de, olli.sipila@helsinki.fi
[3] School of Physics and Astronomy, University of Leeds, Leeds LS2 9JT, UK
[4] Dept. of Physics, University of Florida, Gainesville, FL 32611, USA; jt@astro.ufl.edu
[5] University of Bordeaux, LAB, UMR 5804, F-33270, Floirac, France; wakelam@obs.u-bordeaux1.fr
[6] CNRS, LAB, UMR 5804, F-33270, Floirac, France
*Received 2014 June 24; accepted 2015 February 23; published 2015 May 6*

## ABSTRACT

The deuterium fraction, $[N_2D^+]/[N_2H^+]$, may provide information about the ages of dense, cold gas structures, which are important for comparing dynamical models of cloud core formation and evolution. Here we introduce a complete chemical network with species containing up to three atoms, with the exception of the oxygen chemistry, where reactions involving $H_3O^+$ and its deuterated forms have been added, significantly improving the consistency with comprehensive chemical networks. Deuterium chemistry and spin states of $H_2$ and $H_3^+$ isotopologues are included in this primarily gas-phase chemical model. We investigate the dependence of deuterium chemistry on these model parameters: density ($n_H$), temperature, cosmic ray ionization rate, and gas-phase depletion factor of heavy elements ($f_D$). We also explore the effects of time-dependent freeze-out of gas-phase species and the dynamical evolution of density at various rates relative to free-fall collapse. For a broad range of model parameters, the timescales to reach large values of $D_{\rm frac}^{N_2H^+} \gtrsim 0.1$, observed in some low- and high-mass starless cores, are relatively long compared to the local free-fall timescale. These conclusions are unaffected by introducing time-dependent freeze-out and considering models with evolving density, unless the initial $f_D \gtrsim 10$. For fiducial model parameters, achieving $D_{\rm frac}^{N_2H^+} \gtrsim 0.1$ requires collapse to be proceeding at rates at least several times slower than that of free-fall collapse, perhaps indicating a dynamically important role for magnetic fields in supporting starless cores and thus the regulation of star formation.

*Key words:* astrochemistry – ISM: clouds – stars: formation

## 1. INTRODUCTION

Deuterated molecules are useful diagnostic tools for studying the cold and dense environments where stars are born. This has been demonstrated in low-mass star-forming regions (e.g., Caselli 2002; Bacmann et al. 2003; Crapsi et al. 2005, 2007; Emprechtinger et al. 2009; Friesen et al. 2010), as well as in regions thought to be precursors of massive stars and stellar clusters (e.g., Fontani et al. 2006, 2009, 2011; Pillai et al. 2007, 2012). Deuterated species can be used to infer the elusive electron fraction $x(e)$ (e.g., Guelin et al. 1977; Wootten et al. 1979; Caselli et al. 1998; Bergin et al. 1999; Dalgarno 2006, although the equations in these papers need to be modified to include the doubly and triply deuterated forms of $H_3^+$) and the age of molecular clouds (Pagani et al. 2011, 2013; Brünken et al. 2014). Electron fraction and cloud age are two important parameters for shedding light on the dynamical evolution of star-forming regions, as the ambipolar diffusion timescale is directly proportional to $x(e)$ (e.g., Shu et al. 1987) and the age can put stringent constraints on the mechanism(s) regulating cloud core formation (e.g., magnetic fields, turbulence, and shocks). However, variations in cosmic-ray (CR) ionization rate, volume density, kinetic temperature, rates of molecular freeze-out onto dust grain surfaces, and the ortho-to-para ratio of $H_2$ make attempts to fix these values rather uncertain, especially for regions with poorly known physical structures.

Extensive effort has been spent on understanding the chemistry in starless/pre-stellar cores (e.g., Flower et al. 2006; Pagani et al. 2009, hereafter P09; Parise et al. 2011; Aikawa et al. 2012; Sipilä et al. 2013). However, since they focused on specific aspects of modeling, those studies were limited by either the incompleteness of reactions or the narrow range of physical conditions. In this paper we use a complete reduced network with up-to-date rate coefficients, and uniformly explore the parameter space without any prior bias about the dynamical history, as this depends on poorly known physical quantities such as magnetic fields and turbulence. This parameter space exploration is needed to understand the dependence of the chemical composition (in particular the abundance of deuterated molecules) on basic physical properties and parameters, and to help the interpretation of observational data. It is the first time such an exploration has been done with complete spin-state reactions.

Recently, Pagani et al. (2013) investigated these effects by coupling hydrodynamics with chemistry. They developed an astrochemical model to derive the age of low-mass cores and extensively discussed the role of o-$H_2$. However, they used a relatively limited set of reactions: their chemical network was first based on that of Lesaffre et al. (2005), with 120 reactions and 35 species; then later improved by P09 to include about 400 reactions. The P09 network ignores reactions with rate coefficients below $10^{-15}$ cm$^{-3}$ s$^{-1}$, thus no radiative association reactions, important for carbon chemistry, are included. Furthermore, their model does not fully track the N chemistry ($N_2$ abundance is a parameter), so they are not able to predict absolute abundances of $N_2H^+$ and $N_2D^+$.

In this paper, we first introduce a more complete chemical network and describe our methods of following chemical

evolution (Section 2). In Section 3 we present our results for determining the chemical age of cloud cores by the deuterium fraction of $N_2H^+$. This is similar to the approaches of P09 and Pagani et al. (2013), but extended to cover a broader range of conditions, including those relevant to high-mass star-forming regions that may contain massive starless cores (e.g., Tan et al. 2013). Furthermore, we consider a range of simple parameterized collapse rates relative to that of free-fall collapse. The implications of our results are discussed in Section 4, including detailed comparison with the results of P09 and Pagani et al. (2013). Conclusions are summarized in Section 5.

## 2. METHODS

### 2.1. Fiducial Chemical Network

Our model is based on the network first described in Vastel et al. (2012) (hereafter V12), who used the chemistry results to interpret ground-based and *Herschel Space Observatory* observations of deuterated isotopologues of $H_3^+$ toward a pre-stellar core (see description in their Section 3.3). The V12 code was originally built starting from a complete reaction network that included only molecules with up to three atoms in size, extracted from the Nahoon network (Wakelam et al. 2012), which is available in the KIDA[7] database (Oct. 2010 version). The reduced network only includes the elements H, D, He, O, C, and N. This simplified network still allows us to follow easy-to-observe species in the gas phase, such as $N_2H^+$, $HCO^+$, and their deuterated forms. The reduced network includes the spin states of $H_2$, $H_3^+$, and their deuterated isotopologues, following prescriptions of Walmsley et al. (2004), Flower et al. (2006), Hugo et al. (2009), P09, and Sipilä et al. (2010), and selecting the most recent values for the rate coefficients from the 2010 KIDA database.

We have made five main improvements to the V12 network: (1) The dissociative recombination rates of all the forms of $H_3^+$ have been calculated through the interpolation of Table B.1 of P09. (2) Rate coefficients have been updated and recombination reactions of $C^+$, $N^+$, and $O^+$ onto negatively charged dust grains have been added, following the more recent 2011 KIDA network. (3) Bugs in the duplication routine used to construct the V12 network have been corrected. In particular, we adjusted the branching ratio of reactions such as

$$HD + CO^+ \rightarrow H + DCO^+ \quad (1)$$

and

$$HD + CO^+ \rightarrow D + HCO^+, \quad (2)$$

which is now a half of that of the following reaction from KIDA:

$$H_2 + CO^+ \rightarrow H + HCO^+. \quad (3)$$

(4) We checked our network against that of Sipilä et al. (2013) (hereafter S13) to make sure that spin-state rules were followed. This implied the elimination of some reactions, such as charge exchange reactions involving spin changes; the elimination of reactions of the type

$$H_2O + H^- \rightarrow o\text{-}H_2 + OH^-, \quad (4)$$

as in cold gas it is assumed that only p-$H_2$ can form in reactions containing only reactants other than $H_2^+$, $H_2$, and $H_3^+$; and the elimination of a few reactions built by the V12 duplication code that did not follow Oka (2004) spin rules, such as

$$p\text{-}H_2 + p\text{-}D_2^+ \rightarrow H + o\text{-}D_2H^+. \quad (5)$$

(5) Because of its importance for oxygen chemistry, we include $H_3O^+$ and its deuterated isotopologues, as well as all reactions involving species that are present in our network. The inclusion of $H_3O^+$ significantly improves the overall agreement with S13. The abundances of electrons, water, CO, $HCO^+$, $DCO^+$, $N_2$, $N_2H^+$, $N_2D^+$ and (the most important species in the network, as the deuterium fraction is typically measured through the $N_2D^+/N_2H^+$ and/or $DCO^+/HCO^+$ column density ratios) are always within a factor of 2 when compared to S13 network. This is also true for deuterium fraction and its equilibrium timescale (defined and studied later in Section 3.2). We did not include the surface chemistry described in S13, since there are large uncertainties involved, while not significantly impacting the gas-phase chemistry of $H_3^+$, $HCO^+$, $N_2H^+$, and their deuterated forms in cold regions (see Section 3.5). However, the surface formation of p-$H_2$, o-$H_2$, HD, p-$D_2$, and o-$D_2$ are included in our network. The rates have been calculated following Le Petit et al. (2002). The ortho-to-para ratio upon surface formation has been assumed equal to the statistical value of 3 for $H_2$ and 2 for $D_2$. Neutral and negatively charged grains are considered. Coulomb focusing was taken into account for reactions involving positively charged ions on negatively charged grains (Draine & Sutin 1987). Our fiducial chemical network now includes 3232 reactions involving 132 different species. The network will be publicly available via the KIDA database.

Our first treatment of molecular freeze-out involves an approximation of reducing the initial elemental abundances of species heavier than He by a "depletion factor," $f_D$ ( = 10 for the fiducial model, fixed in each run). Below, we also describe an extension of this simple approximation to include time-dependent depletion and desorption (Section 2.2).

### 2.2. Time-Dependent Depletion/Desorption

The inclusion of time-dependent depletion and desorption rates of the heavier elements adds additional uncertainty and complexity to the modeling (which is why in the fiducial network, above, depletion factor is treated as a controllable parameter). However, in order to gain a basic insight into the potential effects of these more complex processes, we developed a second network that includes freeze-out and desorption of neutral species, following Hasegawa et al. (1992) and Hasegawa & Herbst (1993). Hereafter we refer to this as the TDD network. Three types of reactions are implemented: (a) sticking onto dust grains; (b) thermal evaporation; (c) CR induced evaporation. Binding energies and sticking coefficients are the same as those used in Garrod et al. (2007). Altogether there are 153 new reactions added into the TDD network.

### 2.3. Fiducial Initial Conditions and Model Parameters

We choose the following fiducial initial conditions and model parameters (see also Table 1). The density is expressed

[7] http://kida.obs.u-bordeaux1.fr/

**Table 1**
Fiducial Parameter Values

| Parameter | Description | Fiducial Value |
|---|---|---|
| $n_H$ | number density of H nuclei | $1.0 \times 10^5$ cm$^{-3}$ |
| $T$ | temperature | 15 K |
| $\zeta$ | CR ionization rate | $2.5 \times 10^{-17}$ s$^{-1}$ |
| $f_D$ | depletion factor | 10 |
| $G_0$ | ratio to Habing field | 1 |
| $A_V$ | visual extinction | 30 mag |
| DGR[a] | dust-to-gas mass ratio | $7.09 \times 10^{-3}$ |
| $a_0$ | dust particle radius | $1.0 \times 10^{-5}$ cm |
| $\rho_{GRAIN}$ | dust grain density | 3.0 g cm$^{-3}$ |

**Note.**
[a] Following Draine (2011).

**Table 2**
Fiducial Initial Elemental Abundances

| Species | Abundance ($n_{species}/n_H$) |
|---|---|
| p-$H_2$ | $1.25 \times 10^{-01}$ |
| o-$H_2$ | $3.75 \times 10^{-01}$ |
| HD | $1.50 \times 10^{-05}$ |
| He | $1.00 \times 10^{-01}$ |
| N | $2.10 \times 10^{-06}$ |
| O | $1.80 \times 10^{-05}$ |
| C | $7.30 \times 10^{-06}$ |
| GRAIN0 | $1.32 \times 10^{-12}$ |

via the number density of H nuclei, $n_H = 10^5$ cm$^{-3}$, gas temperature, $T = 15$ K, and heavy element depletion factor, $f_D = 10$. The choices of these fiducial values are motivated by observations of both low- and high-mass pre-stellar cores (e.g., Ward-Thompson et al. 1999; Crapsi et al. 2005, 2007; Pillai et al. 2006; Hernandez et al. 2011; Ragan et al. 2011; Butler & Tan 2012). The CR ionization rate, $\zeta = 2.5 \times 10^{-17}$ s$^{-1}$, is adopted from van der Tak & van Dishoeck (2000).

The fiducial visual extinction, $A_V$, is set to 30 mag, a value large enough that photochemistry is unimportant for our adopted radiation field (standard Habing field, $G_0 = 1$). We assume that refractory metals of low ionization potential (such as Mg and Fe) and polycyclic aromatic hydrocarbons (PAHs), important for the ionization structure, are not present in the gas phase because of freeze-out onto dust grains, a reasonable assumption in cold molecular clouds (see Caselli et al. 1998; Wakelam & Herbst 2008, for the effects of metals and PAHs, respectively, on the chemical structure of molecular clouds). The dust-to-gas mass ratio, grain radius, and grain density are taken from the original Nahoon model and represent the fiducial values typically adopted in chemical models.

The fiducial initial fractional abundances of elements, with respect to total H nuclei are listed in Table 2. For simplicity, all species are assumed to be in atomic form, except for H and D. Deuterium is initially assumed to be all in HD, with a fractional abundance adopted from the measurement of the elemental [D]/[H] ratio measured in the Galactic interstellar medium ([D]/[H] $\sim 1.5 \times 10^{-5}$; e.g., Oliveira et al. 2003). Below, we also investigate the effects of changing these initial chemical states, finding that our main results are quite insensitive to these choices.

The fiducial initial ortho-to-para $H_2$ ratio, $OPR^{H_2}$, is set to its statistical value of 3, assumed to be obtained in the process of $H_2$ formation on dust grain surfaces. This choice does impact deuterium chemistry, and so below we do consider the effects of a range of initial values.

## 3. RESULTS

### 3.1. The Fiducial Model

Figure 1 shows the fractional abundances ([species] = $n_{species}/n_H$) of important species as a function of time in the fiducial model, i.e., the fiducial network with fiducial initial conditions. As the gas evolves under these cold, dense conditions, the deuteration becomes active through the exothermic reaction (only true with respect to para states of reactants and products; Pagani et al. 1992):

$$\text{p-}H_3^+ + HD \rightleftharpoons \text{p-}H_2D^+ + \text{p-}H_2 + 232\ \text{K}. \quad (6)$$

$H_2D^+$ can cede a deuteron to major neutral species, such as CO and $N_2$, producing $DCO^+$ and $N_2D^+$, respectively. As a consequence, the deuterium fraction (i.e., defined by the abundance ratios $[N_2D^+]/[N_2H^+]$, $[DCO^+]/[HCO^+]$) starts to overcome the cosmic abundance of deuterium. Hereafter, we denote the deuterium fraction of a certain species as $D_{frac}^{species}$ (e.g., $[N_2D^+]/[N_2H^+] \equiv D_{frac}^{N_2H^+}$) and the spin-state ratio as $OPR^{species}$ (e.g., $[\text{o-}H_2]/[\text{p-}H_2] \equiv OPR^{H_2}$). We will focus on $D_{frac}^{N_2H^+}$ in our study, since $HCO^+$ suffers more from depletion than $N_2H^+$, so that $D_{frac}^{N_2H^+}$ is a better tool for tracing the inner, denser regions of starless/pre-stellar cores (Caselli et al. 2002; Crapsi et al. 2005).

The deuterium fraction, shown in Figure 2, increases significantly only at times later than $\sim 10^5$ yr, when the abundance of o-$H_2$ starts to drop. Deuteration is suppressed by o-$H_2$, which drives reaction (6) backwards, as originally pointed out by Forets et al. (1991) (for p-$H_2D^+$) and Pagani et al. (1992) (for o-$H_2D^+$), and later discussed by Flower et al. (2006), P09, and Pagani et al. (2011). The conversion of o-$H_2$ to p-$H_2$ mainly proceeds through the reactions of o-$H_2$ with $H^+$ and $H_3^+$. Figure 2 shows how $OPR^{H_2}$ and $D_{frac}^{N_2H^+}$ change together in the fiducial model: as expected, $D_{frac}^{N_2H^+}$ goes up as $OPR^{H_2}$ drops. After reaching the equilibrium steady-state at about 2 million years, $D_{frac}^{N_2H^+}$ has increased by about 4 orders of magnitude relative to the cosmic deuterium to hydrogen abundance ratio, while $OPR^{H_2}$ has dropped by more than 3 orders of magnitude. One can also see from Figure 1 that all species reach steady state when $OPR^{H_2}$ does. These results emphasize that $OPR^{H_2}$ is crucial for cold gas chemistry in general, for deuterium fractionation in particular and for the chemical timescale (see Section 3.3.2).

One thing to note is that in our model, the abundance of heavy molecules such as CO and $N_2$ increases with time (Figure 1). As CO and $N_2$ are both important destruction partners of $H_3^+$ and its deuterated isotopologues, their increasing abundance would tend to reduce that of these species. However, the countervailing effect of the decreasing abundance of o-$H_2$ is more dominant. At the physical conditions of the fiducial model, as time proceeds, species like CO should suffer from increasing amounts of freeze-out onto dust grains (e.g., Caselli et al. 1999). We have not included any differential freeze-out mechanism for CO and $N_2$, as laboratory work has found similar sticking coefficients and

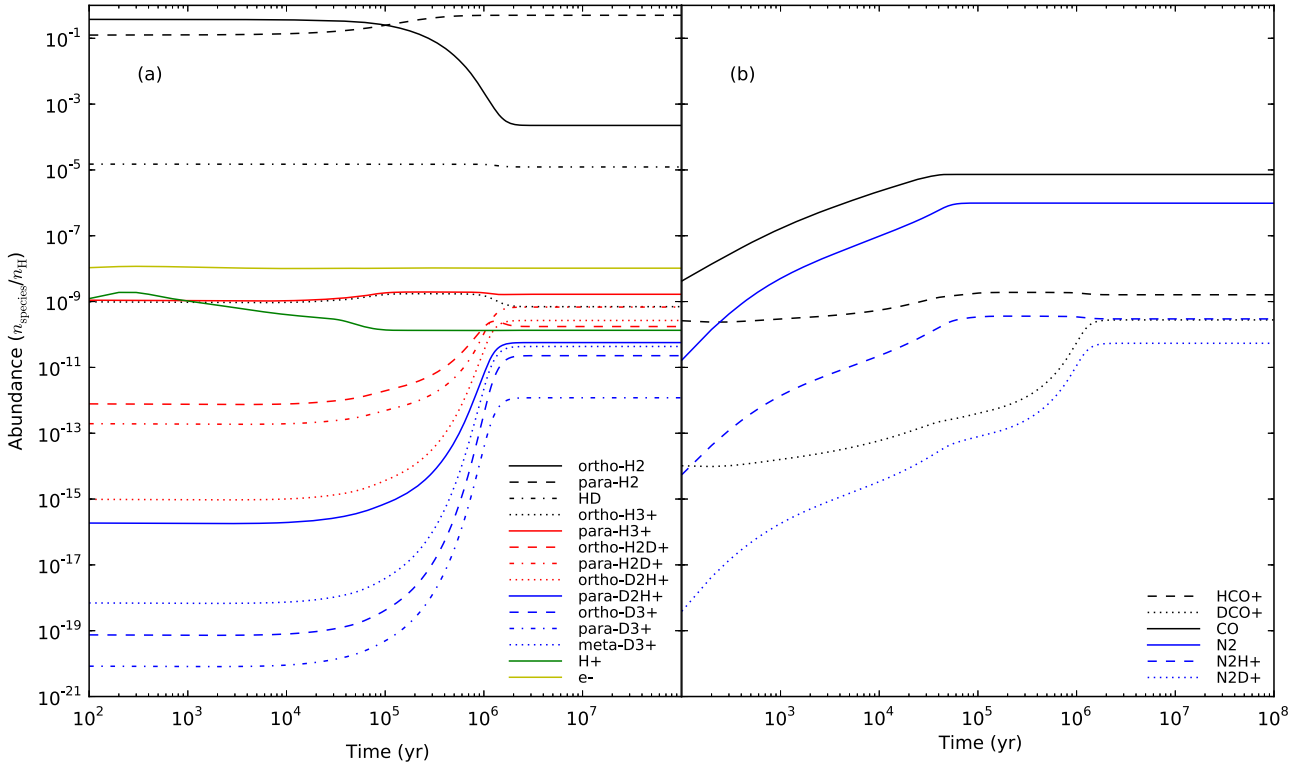


**Figure 1.** Time evolution of the fractional abundances of important species in the fiducial model with $n_H = 1.0 \times 10^5$ cm$^{-3}$, $T = 15$ K, $\zeta = 2.5 \times 10^{-17}$ s$^{-1}$, $f_D = 10$, $G_0 = 1$, and $A_V = 30$ mag. (a): hydrogen species, including $H_2$, $H_3^+$, and their deuterated isotopologues (plus spin states), and electrons. (b): species of interest in this study, especially $N_2D^+$, $N_2H^+$, and their progenitor $N_2$.

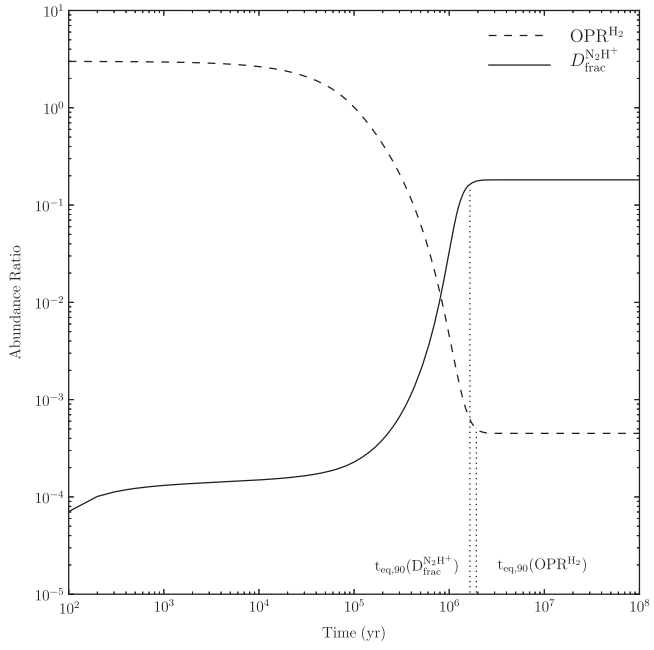


**Figure 2.** Time evolution of $OPR^{H_2} \equiv$ [o-$H_2$]/[p-$H_2$] and $D_{frac}^{N_2H^+} \equiv [N_2D^+]/[N_2H^+]$ in the fiducial model. Two dotted lines mark the times when these quantities approach within 10% of their final equilibrium values ($t_{eq,90}$).

binding energies for the two molecules (Bisschop et al. 2006). Recall also that this fiducial network assumes a fixed, heavy element-independent depletion factor that is present from the initial condition. The effects of relaxing this assumption are investigated in Section 3.5.

With these caveats in mind, we note from Figure 1 that the $N_2H^+$/CO ratio increases with time, up to a few times $10^5$ yr, when the $N_2H^+$ abundance reaches steady state, as $N_2$, the precursor molecule to $N_2H^+$, forms more slowly than CO, via neutral–neutral reactions rather than ion–neutral reactions (see also Hily-Blant et al. 2010).

### 3.2. The Deuteration Timescale

Studies have suggested a theoretical relation between the deuterium fraction and the evolutionary stage in low-mass cores (Caselli 2002; Crapsi et al. 2005; Pagani et al. 2013), with the level of deuteration rising with increasing age and density of the starless core, before then falling once a protostar forms and starts to heat its natal envelope. Fontani et al. (2011) have examined a similar relation in massive cores, and their findings support the use of deuterium fraction as an evolutionary indicator for massive starless and star-forming cores.

Here we investigate the absolute timescale for the growth of the deuterium fraction and its implication for the ages of low-mass and massive starless cores. We also examine how the variation of physical properties of the gas, including choices of initial conditions, influences this deuteration timescale, i.e., a chemical timescale. For convenience, when considering the output of our chemical network, we define the equilibrium deuterium fraction, $D_{frac,eq}$ as the average of two adjacent outputs of $D_{frac}$ (separated by $\Delta t = 10^4$ yr) that have a fractional change

$$|\Delta D_{frac}|/D_{frac} < \epsilon, \quad (7)$$

**Table 3**
Equilibrium Abundance Ratios and Timescales for Models with Various Initial Conditions

| Model | $OPR_{eq}^{H_2}$ ($\times 10^{-4}$) | $t_{eq}(OPR^{H_2})$ ($10^6$ yr) | $t_{eq,90}(OPR^{H_2})$ ($10^6$ yr) | $D_{frac,eq}^{N_2H^+}$ | $t_{eq}(D_{frac}^{N_2H^+})$ ($10^6$ yr) | $t_{eq,90}(D_{frac}^{N_2H^+})$ ($10^6$ yr) |
|---|---|---|---|---|---|---|
| Fiducial | 4.51 | 2.98 | 1.93 | 0.181 | 2.68 | 1.65 |
| Atomic D | 4.51 | 2.98 | 1.93 | 0.181 | 2.68 | 1.65 |
| Fully molecular | 4.51 | 2.98 | 1.92 | 0.181 | 2.66 | 1.63 |
| Half N in $N_2$ | 4.51 | 2.98 | 1.92 | 0.181 | 2.66 | 1.63 |
| $OPR^{H_2}(t=0)=3$ | 4.51 | 2.98 | 1.93 | 0.181 | 2.68 | 1.65 |
| $OPR^{H_2}(t=0)=1$ | 4.51 | 2.92 | 1.86 | 0.181 | 2.60 | 1.57 |
| $OPR^{H_2}(t=0)=0.1$ | 4.51 | 2.60 | 1.54 | 0.181 | 2.28 | 1.25 |
| $OPR^{H_2}(t=0)=0.01$ | 4.51 | 2.18 | 1.12 | 0.181 | 1.86 | 0.830 |
| $OPR^{H_2}(t=0)=0.001$ | 4.51 | 1.64 | 0.578 | 0.181 | 1.32 | 0.290 |
| $OPR^{H_2}(t=0)=0.0007$ | 4.51 | 1.48 | 0.429 | 0.181 | 1.16 | 0.152 |
| Maximum $D_{frac}$ model[a] | 1.33 | 0.725 | 0.429 | 0.903 | 0.645 | 0.338 |

**Note.**
[a] See Section 3.4.6.

with a choice of $\epsilon = 5 \times 10^{-5}$. In practice, we run the model for $10^8$ yr and then search backward in time for when this condition is satisfied. We denote the timescale to reach the equilibrium condition defined by Equation (7) as $t_{eq}(D_{frac}^{species})$. The equilibrium value of the ortho-to-para ratio of $H_2$, $OPR_{eq}^{H_2}$, is defined in a similar way, and the timescale is denoted $t_{eq}(OPR^{H_2})$. In practice, since the evolution of $D_{frac}^{N_2H^+}$ and $OPR_{eq}^{H_2}$ are very slow as they approach equilibrium (e.g., Figure 2), we also define a more representative equilibrium timescale $t_{eq,90}(D_{frac}^{N_2H^+})$ as the time when $D_{frac}^{N_2H^+}$ increases to 90% of $D_{frac,eq}^{N_2H^+}$. In a similar way, we define $t_{eq,90}(OPR^{H_2})$ as the time when $OPR^{H_2}$ decreases to $OPR_{eq}^{H_2}/0.90$.

We will compare these chemical timescales to physical timescales, in particular the local free-fall timescale, $t_{ff}$, which, for a uniform density core, is

$$t_{ff} = \left(\frac{3\pi}{32G\rho}\right)^{1/2} = 1.39 \times 10^5 \left(\frac{n_H}{10^5\ cm^{-3}}\right)^{-1/2} \text{yr}. \quad (8)$$

Note that this timescale is evaluated with respect to the current density of a core, predicting how long it will take in the future to collapse to a very high density state in the absence of any internal pressure support. However, this timescale is also an approximate estimate for the minimum amount of time that the core has existed at densities similar to its current value, since if contraction is driven by self-gravity we do not expect evolution in core properties to be proceeding on timescales shorter than the local free-fall time.

Furthermore, depending on the degree of turbulent and magnetic field support, the contraction could be proceeding at rates much slower than that of free-fall collapse. Thus, in Section 3.6, we will also consider models in which the density evolves continuously at various rates relative to the local free-fall time.

Note that the deuteration timescale refers to the age of a core, which in our fiducial modeling is the time spent at the given constant density. In the evolving density models, the deuteration timescale is the time the core has spent evolving from a particular lower density initial condition to the current density. When comparing to observations, one has to take into account that dense cores have been evolving from lower densities, so models with evolving density structures are important for constraining the rates of collapse from the measured abundances of deuterated molecules.

The first line of Table 3 lists equilibrium abundance ratios and timescales for the fiducial model, i.e., with $n_H = 10^5\ cm^{-3}$. The deuteration timescale $t_{eq,90}(D_{frac}^{N_2H^+})$ is $\simeq 12 t_{ff}$. Thus, if a starless core were to be observed with physical and environmental properties equal to the fiducial model, and $D_{frac} \gtrsim 0.1$, then our modeling implies it would need to be substantially older than its current local $t_{ff}$, assuming it had started with our adopted initial conditions, including the initial OPR of $H_2$.

### 3.3. Effect of Initial Conditions on the Deuteration Timescale

#### 3.3.1. Initial Elemental Abundances

As shown in Table 2, the fiducial model starts with H in molecular form, D in HD, while He, C, N, and O are in atomic form. However, when dense cores form in molecular clouds, a large fraction of CO and maybe $N_2$ should already be present (see also Li et al. 2013). There is some evidence that a significant fraction of the nitrogen is still in atomic form in dense cores due to the slow conversion from N to $N_2$, but the exact amount is unclear (Hily-Blant et al. 2010). As different initial abundances could impact $D_{frac,eq}^{species}$ and $t_{eq,90}(D_{frac}^{species})$, we quantify these effects considering 3 variations to the fiducial model descibed in Section 2.3: (1) "atomic D," where D is in atomic form, compared to the fiducial model, assuming that $H_2$ is in molecular form; (2) "fully molecular," where everything starts in molecular form (all N in $N_2$, all C in CO, with the leftover oxygen left in atomic form); and (3) "half N in $N_2$," where half of the nitrogen is left in atomic form compared to the "fully molecular" case.

Figure 3 shows the results of these tests, focusing on the effects on the time evolution of $D_{frac}^{N_2H^+}$ and $OPR^{H_2}$. Table 3 lists the equilibrium ratios and timescales. The choice of initial atomic versus molecular abundances has no effect on the

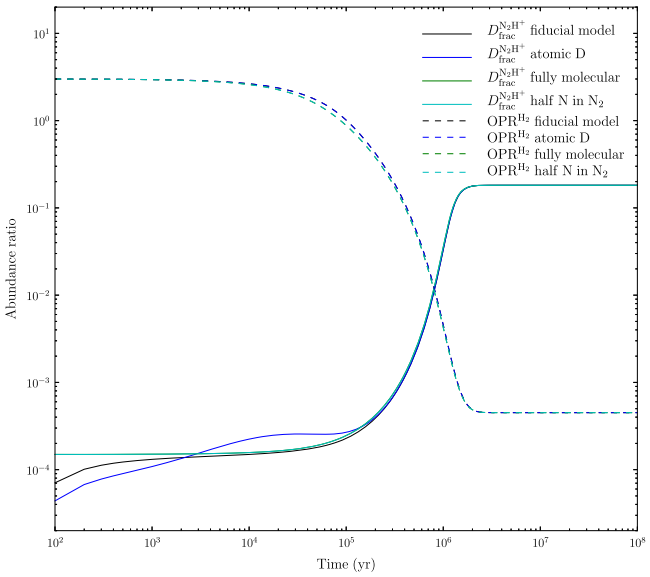


**Figure 3.** Time evolution of $\rm OPR^{H_2}$ and $D_{\rm frac}^{\rm N_2H^+}$ with four sets of initial elemental abundances. See Section 3.3.1 for the description of these sets. The equilibrium ratios and timescales are summarized in Table 3.

equilibrium abundance ratios and has little effect ($\lesssim$1%) on the timescales.

#### 3.3.2. *Initial* $\rm OPR^{H_2}$

Another poorly constrained, but crucial, parameter is the initial $\rm OPR^{H_2}$. There are only a few studies yielding observational constraints: in diffuse clouds, Crabtree et al. (2011) measured $\rm OPR^{H_2} \simeq 0.3$–0.8; in the pre-stellar core L183, P09 derived $\rm OPR^{H_2} \simeq 0.1$ (see also Pagani et al. 2011), while Troscompt et al. (2009) estimated $\rm OPR^{H_2} < 1$, and Maret & Bergin (2007) estimated $\rm OPR^{H_2} \sim 0.015$ in the starless Bok globule B68 (see also discussion in Flower et al. 2006; S13). Evidently, different environmental conditions strongly impact $\rm OPR^{H_2}$ (as also deduced by Caselli et al. 2008, in their study of o-$H_2D^+$ in star-forming regions).

Our fiducial model starts with $\rm OPR^{H_2} = 3$, which implies that all $H_2$ molecules are initially in their statistical spin ratio, as expected if they have just been formed on the surface of dust grains, i.e., if the molecular cloud is very young. However, this may not be the case, based on the abovementioned observations in diffuse clouds and if cloud cores form at a later stage compared to the formation of the parent molecular cloud. To explore this, we consider the effect of different initial $\rm OPR^{H_2}$ values in the fiducial model. Figure 4 shows their effects on the time evolution of $\rm OPR^{H_2}$ and $D_{\rm frac}^{\rm N_2H^+}$. The different initial $\rm OPR^{H_2}$ values have little effect on both $\rm OPR_{eq}^{H_2}$ and $D_{\rm frac,eq}^{\rm N_2H^+}$, but the timescales to reach equilibrium are changed (as also found by Pagani et al. 2011, see their Figure 2). Since the $\rm OPR_{eq}^{H_2}$ is $4.51 \times 10^{-4}$, the lower the initial $\rm OPR^{H_2}$, the sooner chemical equilibrium will be reached. We find $t_{\rm eq,90}(D_{\rm frac}^{\rm N_2H^+})$ becomes similar to $t_{\rm ff}$ if $\rm OPR^{H_2}$ is initially 0.001 or lower. This is also summarized in Table 3. These results suggest that we should in general consider the possible effects of starting with much lower values of the initial $\rm OPR^{H_2}$ than the fiducial value of 3 (although initial values lower than 0.1 are not consistent with $DCO^+$ observations, as discussed in Pagani et al. 2011).

### 3.4. *Effect of Starless Core Physical and Environmental Properties on the Deuteration Timescale*

Here we present a parameter space exploration to see how different physical conditions impact the chemical evolution of gas in starless cores. We will first assume an initial $\rm OPR^{H_2} = 3$ (results for $\rm OPR^{H_2} = 1$, 0.1, 0.01 are discussed below in Section 3.4.5). Then, we vary four parameters: the H number density $n_{\rm H}$ from $10^3$ to $10^7$ cm$^{-3}$, the temperature $T$ from 5 to 30 K, the CR ionization rate $\zeta$ from $10^{-18}$ to $10^{-15}$ s$^{-1}$, and the gas phase depletion factor $f_D$ from 1 to 1000 ($f_D = 1$ implies no depletion).[8] These ranges of parameter space are chosen to cover the conditions expected for both low and high-mass starless cores (e.g., Bergin & Tafalla 2007; Tan et al. 2014).

Figure 5 shows the effect on the time evolution of $\rm OPR^{H_2}$ and $D_{\rm frac}^{\rm N_2H^+}$ of varying these four parameters. In general, $n_{\rm H}$ and $T$ have a greater influence on $D_{\rm frac,eq}^{\rm N_2H^+}$, while $\zeta$ and $f_D$ have an effect on both $D_{\rm frac,eq}^{\rm N_2H^+}$ and $\rm OPR^{H_2}$. This implies that the physical environment plays an important role in dense core chemistry. It is thus crucial to have good observational constraints on these properties when trying to model observed cores.

Figure 6 shows the variation of the equilibrium ratios and timescales of $\rm OPR^{H_2}$ (upper 2 rows) and $D_{\rm frac}^{\rm N_2H^+}$ (lower 2 rows). Note that the variation of the equilibrium time of $D_{\rm frac}^{\rm N_2H^+}$ (fourth row) is very similar to that of $\rm OPR^{H_2}$ (second row), as explained in Section 3.1. In the following, we summarize their dependence on each physical quantity, with emphasis on $D_{\rm frac}^{\rm N_2H^+}$ and $t_{\rm eq,90}(D_{\rm frac}^{\rm N_2H^+})$.

#### 3.4.1. *Dependence on* $n_{\rm H}$

As shown in panel (i) of Figure 6, a denser core will have a higher $D_{\rm frac,eq}^{\rm N_2H^+}$. The $D_{\rm frac,eq}^{\rm N_2H^+}$ changes by $\sim$ an order of magnitude, from $3.21 \times 10^{-2}$ at $n_{\rm H} = 10^3$ cm$^{-3}$, to $3.51 \times 10^{-1}$ at $n_{\rm H} = 10^7$ cm$^{-3}$.

From panel (m) we see that $t_{\rm eq,90}(D_{\rm frac}^{\rm N_2H^+})$ varies with $n_{\rm H}$ by a factor of $\sim$ 7. Thus, cores with a wide range of densities have similar deuteration timescales, if other conditions are fixed. When $n_{\rm H} \gtrsim 3 \times 10^4$ cm$^{-3}$, $t_{\rm eq,90}(D_{\rm frac}^{\rm N_2H^+})$, and $t_{\rm eq,90}(\rm OPR^{H_2})$ are more than 10 $t_{\rm ff}$ (recall $t_{\rm ff}$ is the local free-fall time at a given density). Thus highly deuterated cores, i.e., with $D_{\rm frac}^{\rm N_2H^+} \gtrsim 0.1$, that have such densities and that also satisfy the other fiducial parameters and assumed initial conditions would, in the context of the assumption of constant (or slow) density evolution, need to be "dynamically old," i.e., have existed at the current density for significantly longer than their local free-fall time. Below, in Section 3.6, we will also place constraints for such cores in the context of dynamically evolving densities.

Panel (m) (and panels n, o, p) also show the ambipolar diffusion timescale, $t_{\rm ad}$, which is expected to be the relevant collapse timescale in magnetically subcritical cores. It is always longer than $t_{\rm ff}$. The ambipolar diffusion timescale is discussed in more detail in Section 4.2.

[8] Note that some small regions of parameter space are not internally self-consistent, e.g., a very cold temperature model with very high CR ionization rate, but our goal here is to first explore the effects of each variable on the deuteration chemistry in isolation before later building self-consistent thermodynamic models.

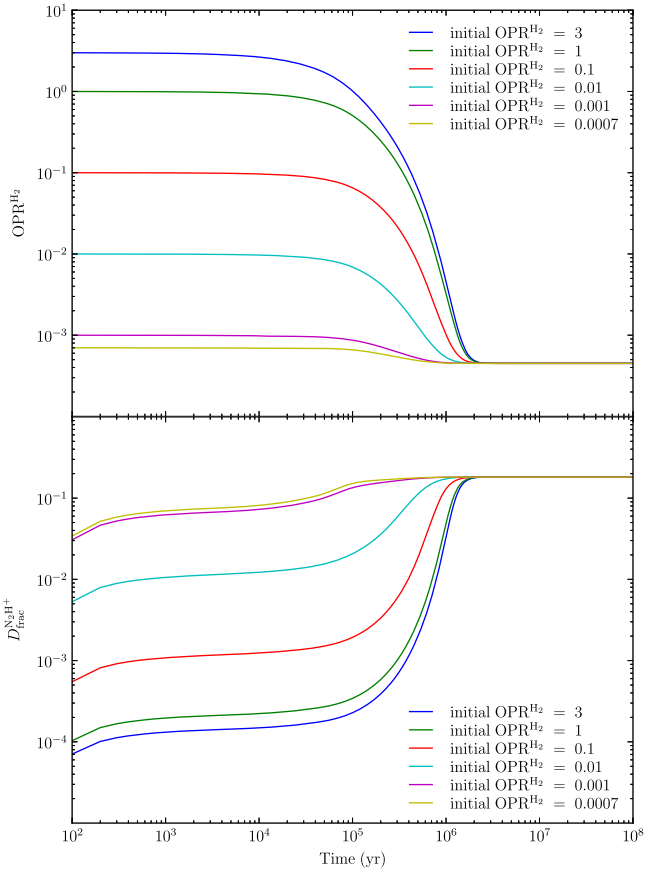


**Figure 4.** Time evolution of $OPR^{H_2}$ (top) and $D_{frac}^{N_2H^+}$ (bottom) under different assumptions of initial $OPR^{H_2}$. We explore initial $OPR^{H_2}$ from 3 (the fiducial model) down to $7 \times 10^{-4}$. Note that $OPR_{eq}^{H_2} \simeq 4.51 \times 10^{-4}$.

#### 3.4.2. Dependence on $T$

As shown in panel (j) of Figure 6, between 5 and 15 K, the $D_{frac,eq}^{N_2H^+}$ profile is quite flat. Above 15 K, $D_{frac,\,eq}^{N_2H^+}$ drops down by almost 2 orders of magnitude as $T$ approaches 30 K. The maximum $D_{frac,eq}^{N_2H^+}$ of 0.19 is achieved at $T = 13$ K. The profile of $t_{eq,90}(D_{frac}^{N_2H^+})$ is also quite flat across the explored temperatures (panel n). We find $t_{eq,90}(D_{frac}^{N_2H^+})$ is always greater than 10 $t_{ff}$ except for the highest temperatures (as is $t_{eq,90}(OPR^{H_2})$). At $T \lesssim 15$ K, $OPR_{eq}^{H_2}$ is well below 0.001, but it goes up quickly at higher temperatures. Regions warmer than 20 K, as, for example, gas in the proximity of young stellar objects, will then experience an increase of the ortho-to-para $H_2$ ratio and thus a drop in the deuterium fraction (in agreement with findings by Fontani et al. 2011 in high-mass star-forming regions and Emprechtinger et al. 2009 in low-mass star-forming regions).

As stated previously, $D_{frac,eq}^{N_2H^+}$ (as well as the deuterium fraction of other deuterated species) is controlled by $OPR_{eq}^{H_2}$. As $T$ goes down to 13 K, $OPR_{eq}^{H_2}$ drops (panel (b) of Figure 6), and $D_{frac,eq}^{N_2H^+}$ (panel (j) of Figure 6) increases. Below 13 K, both $OPR_{eq}^{H_2}$ and $D_{frac,eq}^{N_2H^+}$ become roughly constant. This is because the $H_3^+ + H_2$ reacting system contains reactions with activation energies that convert p-$H_2$ to o-$H_2$, such as:

$$o\text{-}H_3^+ + p\text{-}H_2 \rightarrow p\text{-}H_3^+ + o\text{-}H_2 \quad (9)$$

and

$$o\text{-}H_3^+ + p\text{-}H_2 \rightarrow o\text{-}H_3^+ + o\text{-}H_2. \quad (10)$$

The activation energy barrier of the above reactions are of the order of 100 K. As the temperature drops, the endothermic channels are effectively closed off and the abundances of both p-$H_2$ and o-$H_2$ are controlled mainly by $T$-independent reactions, e.g.,

$$p\text{-}H_2^+ + p\text{-}H_2 \rightarrow p\text{-}H_3^+ + H. \quad (11)$$

Consequently, the $OPR_{eq}^{H_2}$ and $D_{frac,eq}^{N_2H^+}$ become almost independent of $T$.

#### 3.4.3. Dependence on $\zeta$

$D_{frac,eq}^{N_2H^+}$ drops by a factor of 6 as $\zeta$ increases from $10^{-18}$ to $10^{-15}$ s$^{-1}$ (panel k), due to the enhanced electron abundance and the consequent dissociative crated isotopologues of $H_3^+$ (see also Caselli et al. 2008). The highest $D_{frac,eq}^{N_2H^+}$ of 0.33 appears at the lowest $\zeta = 10^{-18}$ s$^{-1}$. This shows the importance for the astrochemical modeling of constraining $\zeta$. Panel (o) shows that $t_{eq,90}(D_{frac}^{N_2H^+})$ changes by more than 2 orders of magnitude within the $\zeta$ range explored. The smallest $t_{eq,90}(D_{frac}^{N_2H^+})$ is only $1.2 \times 10^5$ yr at $\zeta = 10^{-15}$ s$^{-1}$, which is much shorter than $t_{ff}$. However, such high CR ionization rates are not expected to be relevant in typical Galactic star-forming regions (and would also be expected to yield relatively high kinetic temperatures). With moderate $\zeta$ ($\lesssim 10^{-16}$ s$^{-1}$), $t_{eq,90}(D_{frac}^{N_2H^+})$ is significantly greater than $t_{ff}$ ($\gtrsim 7$ $t_{ff}$) at the fiducial density. The dependence of $OPR^{H_2}$ with $\zeta$ is shown in panel (c) and its equilibrium timescale in panel (g).

#### 3.4.4. Dependence on $f_D$

Panel (l) of Figure 6 shows that $D_{frac,eq}^{N_2H^+}$ goes up by more than an order of magnitude as $f_D$ increases from 1 to 1000. This agrees with the expectation that depletion of neutral species, in particular CO and O, the main destruction partners of $H_3^+$ and its deuterated forms, will result in the enhancement of $D_{frac}^{N_2H^+}$ (see also Dalgarno & Lepp 1984). At $f_D = 1000$ we encounter the highest $D_{frac,eq}^{N_2H^+} = 0.93$ in our exploration. Such high values have seldom been observed (e.g., Miettinen et al. 2012). We find $t_{eq,90}(D_{frac}^{N_2H^+})$ decreases with stronger depletion, which is shown in panel (p), although $t_{eq,90}(D_{frac}^{N_2H^+})$ is at least a factor of seven larger than $t_{ff}$ when $f_D \lesssim 100$ at the fiducial density.

An interesting point is whether $D_{frac,eq}^{N_2H^+}$ will keep going up with stronger depletion. We extend our exploration to $f_D = 10^6$, which is shown in Figure 8. We can see in panel (b), that the $D_{frac,eq}^{N_2H^+}$–$f_D$ relation drops moderately at $f_D \sim 2000$. In panel (a), $[H_3^+]$ and $[H_2D^+]$ reach the peak at $f_D \sim 2000$ and drop moderately until $f_D = 10^6$. Besides the destruction partners like CO, electrons can also destroy $H_3^+$

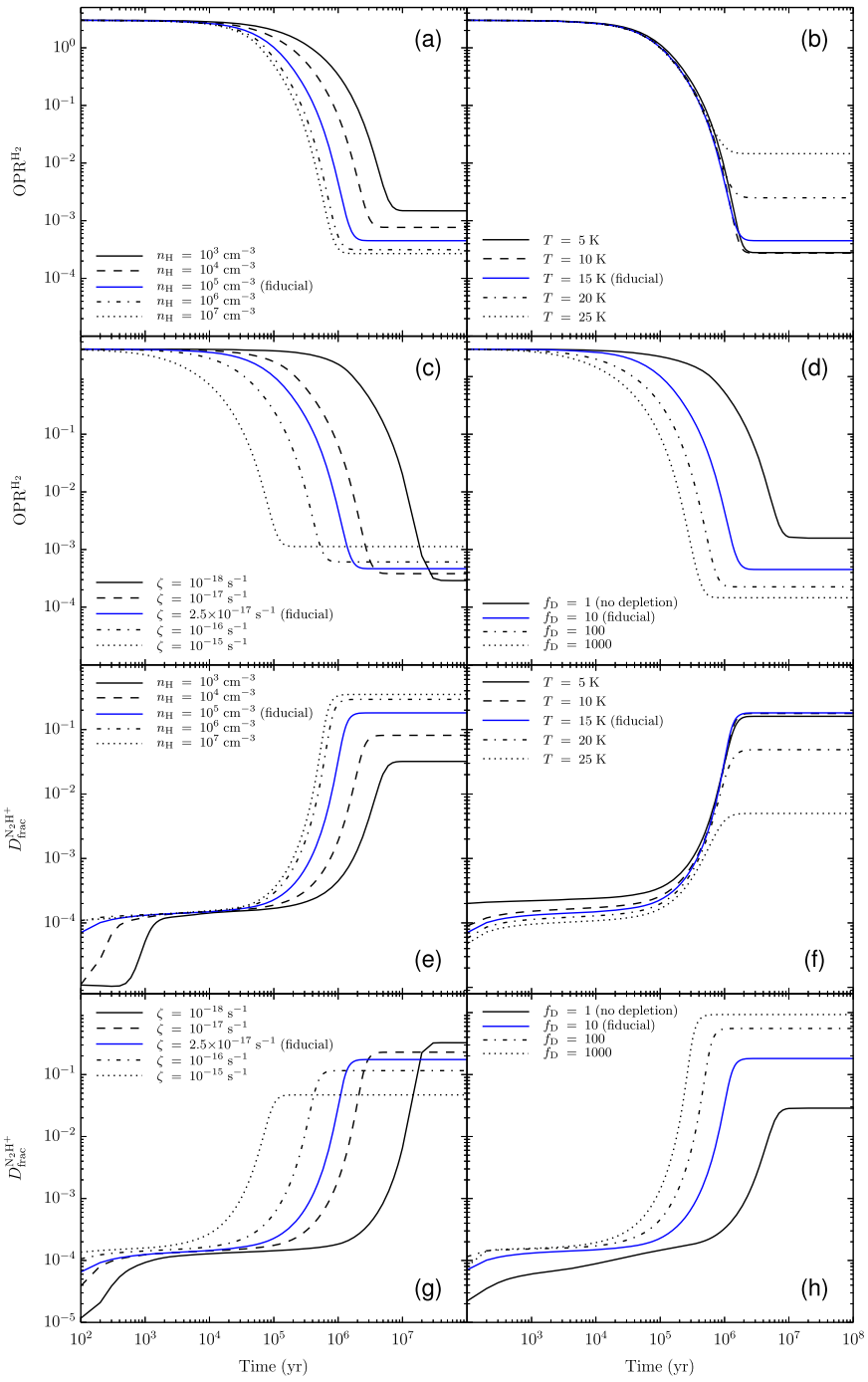


**Figure 5.** Time evolution of $\mathrm{OPR}^{\mathrm{H_2}}$ (panels a to d) and $D_{\mathrm{frac}}^{\mathrm{N_2H^+}}$ (panels e to h) for various densities (a, e), temperatures (b, f), cosmic ray ionization rates (c, g), and depletion factors (d, h). The blue solid lines correspond to the fiducial model (as in Figure 2). In each case of exploring the effect of varying a particular parameter, the other parameter values are set to those of the fiducial model. See Section 3.4 for the complete description of the exploration.

and its deuterated forms. We plot the electron abundance versus $f_D$ in Figure 8(a). As we can see, the electron abundance increases at $f_D \gtrsim 2000$ while $D_{\mathrm{frac,eq}}^{\mathrm{N_2H^+}}$ drops. This supports our expectation that the super-depletion of heavy elements reduces the destruction partners of electrons, so that [e-] can approach a high level, which suppresses the abundances of $H_3^+$ and $H_2D^+$, etc. To confirm this, we remove all dissociative recombination reactions between electron and O-bearing species (~40 reactions. These species contain no nitrogen or carbon)[9] and perform the exploration again. The results are shown in Figure 9. Now

[9] The reason we choose O-bearing species is that we have made another three explorations where we reduce initial [C], [N], [O] independently. We denote the depletion of C, N, O with $f_D$(C), $f_D$(N), $f_D$(O), respectively. We find from the explorations that reducing initial [O] can reproduce the drop in $D_{\mathrm{frac,eq}}^{\mathrm{N_2H^+}}$. So we expect that O-bearing species play the crucial role.

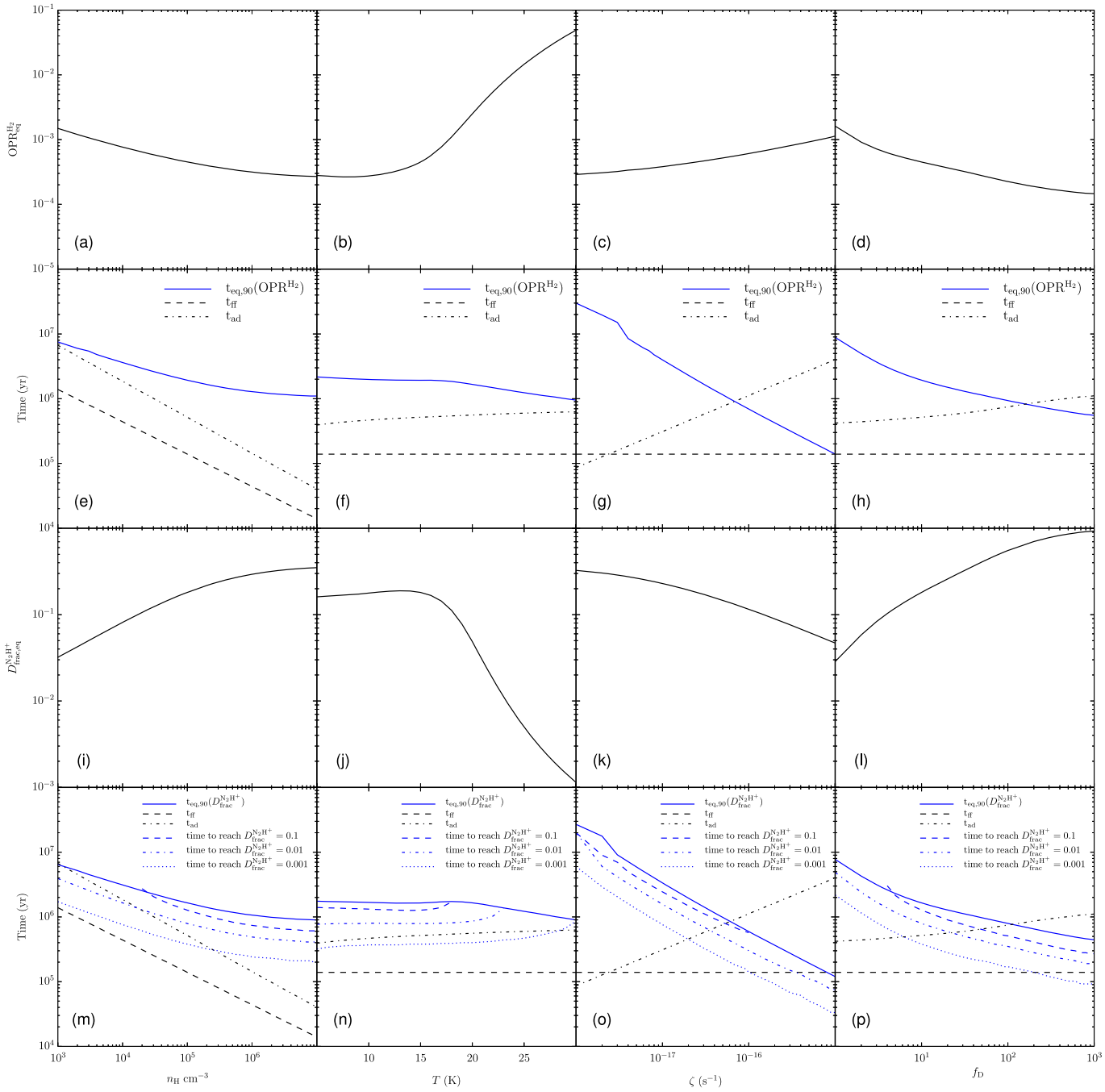


**Figure 6.** Parameter-space exploration of dependence of $OPR_{eq}^{H_2}$ (top row), $t_{eq,90}(OPR^{H_2})$ (second row), $D_{frac,eq}^{N_2H^+}$ (third row), and $t_{eq,90}(D_{frac}^{N_2H^+})$ (bottom row) as a function of density $n_H$ (left column), temperature $T$ (second column), cosmic ray ionization rate $\zeta$ (third column), and depletion factor $f_D$ (right column) (see Section 3.2 for definitions). In the fourth row, we also show the times to reach $D_{frac}^{N_2H^+} = 0.1, 0.01, 0.001$ (missing portions of the lines imply $D_{frac}^{N_2H^+}$ does not reach the value of interest for these conditions). Also shown are free-fall time $t_{ff}$ (Equation (8)) and ambipolar diffusion time $t_{ad}$ (Section 4.2) for comparison with $t_{eq,90}(OPR^{H_2})$ and $t_{eq,90}(D_{frac}^{N_2H^+})$.

we see that the bump of $D_{frac,eq}^{N_2H^+}$ around $f_D \sim 2000$ is gone. $D_{frac,eq}^{N_2H^+}$ simply increases with $f_D$ and reaches a constant value ($\sim$0.7). In panel (a) of Figure 9, because of the reduced number of dissociative reactions, the electron abundance is high at moderate depletion, as compared to Figure 8(a). The [e-] and $D_{frac,eq}^{N_2H^+}$ at extreme $f_D$ approach the same values as those in Figure 8, respectively. These imply that what we see in panel (b) of Figure 8 is the result of the competition between two mechanisms: (1) species like CO can destroy $H_3^+$ and its deuterated forms; (2) O-bearing species consume electrons through dissociative reactions. It turns out that in our exploration of $f_D$ (panel b of Figure 8), mechanism (1) dominates at $f_D \lesssim 2000$, and mechanism (2) dominates at $2000 \lesssim f_D \lesssim 10^4$. At $f_D \gtrsim 10^4$, there are too few O-bearing species consuming electrons, explaining the $D_{frac,eq}^{N_2H^+}$ - $f_D$ relation in Figure 9(b).

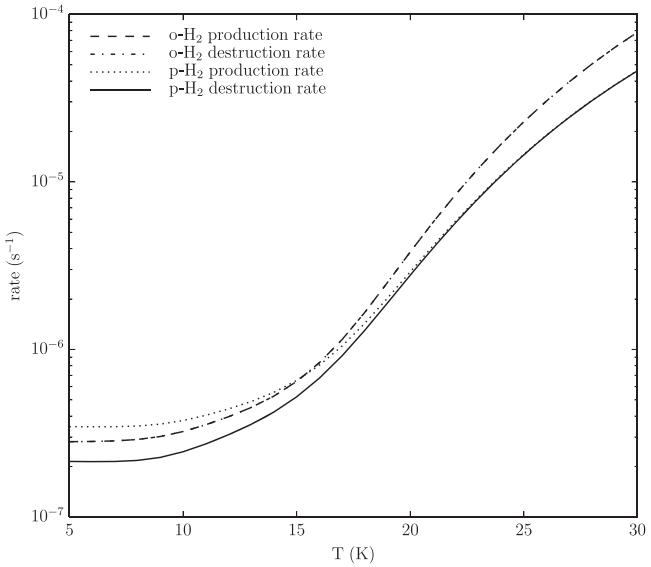


**Figure 7.** Production and destruction rates of o-$H_2$ and p-$H_2$ at equilibrium time step as a function of $T$. See Section 3.4.2.

### 3.4.5. Dependence on Initial $OPR^{H_2}$

The effect of varying the initial $OPR^{H_2}$ on the time evolution of the fiducial model was discussed above in Section 3.3.2. In Figure 10 we show the effect on the deuteration timescale parameter space ($n_H$, $T$, $\zeta$, $f_D$) exploration of starting with $OPR^{H_2} = 1$, 0.1, 0.01, rather than 3.

In general, the effect of a lower starting $OPR^{H_2}$ value is to reduce the timescales needed to reach a given level of $D_{frac}^{N_2H^+}$. However, for most of the parameter space, $t_{eq,90}(D_{frac}^{N_2H^+})$ still remains significantly greater than $t_{ff}$.

### 3.4.6. Highest $D_{frac}^{N_2H^+}$ Predicted in Our Model

High values of $D_{frac}^{N_2H^+}$ have been reported in recent observations of starless cores. Fontani et al. (2011) observed several potential massive starless cores, finding the highest $D_{frac}^{N_2H^+} = 0.7$ in their source Infrared Dark Cloud G2. An even higher value of $D_{frac}^{N_2H^+} = 0.99$ has been reported by Miettinen et al. (2012 though this may be affected by the uncertainties from treating $N_2H^+$ with non-LTE model but $N_2D^+$ with LTE model), toward Orion B9 SMM1. Such high values are not predicted by our fiducial model. However, it is interesting if we combine the explored parameters $n_H$, $T$, $\zeta$, and $f_D$ at the values where $D_{frac,eq}^{N_2H^+}$ peaks ($n_H = 10^7\,cm^{-3}$, $T = 13\,K$, $\zeta = 10^{-18}\,s^{-1}$, $f_D = 1000$) to gauge the maximum level of deuteration that can result from our model (might not be global in core). Equilibrium ratios and timescales are summarized in Table 3. We find $D_{frac}^{N_2H^+}$ goes up to 0.903, while $t_{eq,90}(D_{frac}^{N_2H^+})$ is about 46 $t_{ff}$ ($1.39 \times 10^4$ yr at $n_H = 10^7\,cm^{-3}$). Detailed constraints on the parameter space needed for individual observed sources will be presented in a future study.

### 3.5. Effect of Time-Dependent Depletion/Desorption

In Figure 11 we compare the fiducial model (with constant $f_D = 10$) and the TDD model (with starting values of $f_D = 1$ and $f_D = 10$). Panel (a) shows the time evolution of the fractional abundances of $N_2D^+$, $N_2H^+$, CO, and $N_2$. The time evolution of the abundance of these species show qualitatively similar behaviors in the two models, with modest quantitative differences. We note that the TDD models do not reach equilibrium within $10^8$ yr because of continuing freeze-out, especially of $N_2$. The $N_2D^+$ abundance shows a plateau between $5 \times 10^6$ and $5 \times 10^7$ yr, before dropping together with the $N_2$ abundance.

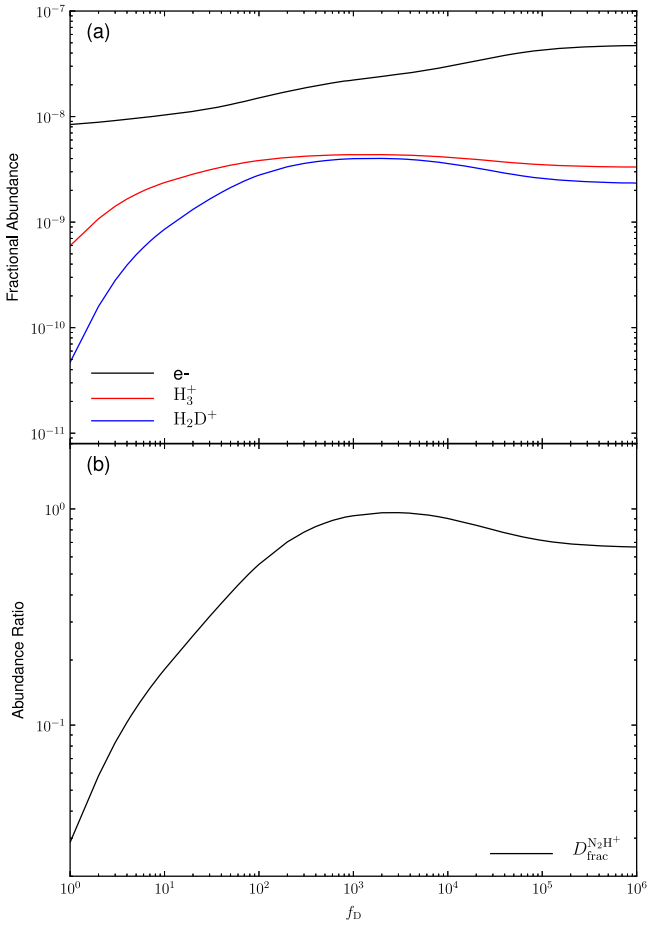


**Figure 8.** (a) Relations between the depletion factor and the fractional abundances (relative to $n_H$) of $H_3^+$, $H_2D^+$, and electron, respectively. The abundances are taken at the equilibrium step of $D_{frac,eq}^{N_2H^+}$. (b) Same as panel (l) in Figure 6, but extended to $f_D = 10^6$.

In panel (b) we compare gas-phase $OPR^{H_2}$ and $D_{frac}^{N_2H^+}$ between the fiducial model and the TDD models. Compared to the fiducial model, the decline of $OPR^{H_2}$ is slower in the $f_D = 1$ TDD model and faster in the $f_D = 10$ TDD model, so that for most of the time evolution, up to $\sim 10^7$ yr, the fiducial models results are bracketed by the TDD models.

Note our simple TDD models do not include surface chemistry, since this opens up even larger uncertainties, which we defer to a future study. As an initial check to see if surface chemistry can have a significant effect, we have examined the S13 models with and without surface reactions. The effect of including surface chemistry within these models on $OPR^{H_2}$ is very minor, and the time evolution of $D_{frac}^{N_2H^+}$ is also largely unaffected. Thus we do not expect our fiducial or TDD model results to be significantly affected by neglecting surface chemistry.

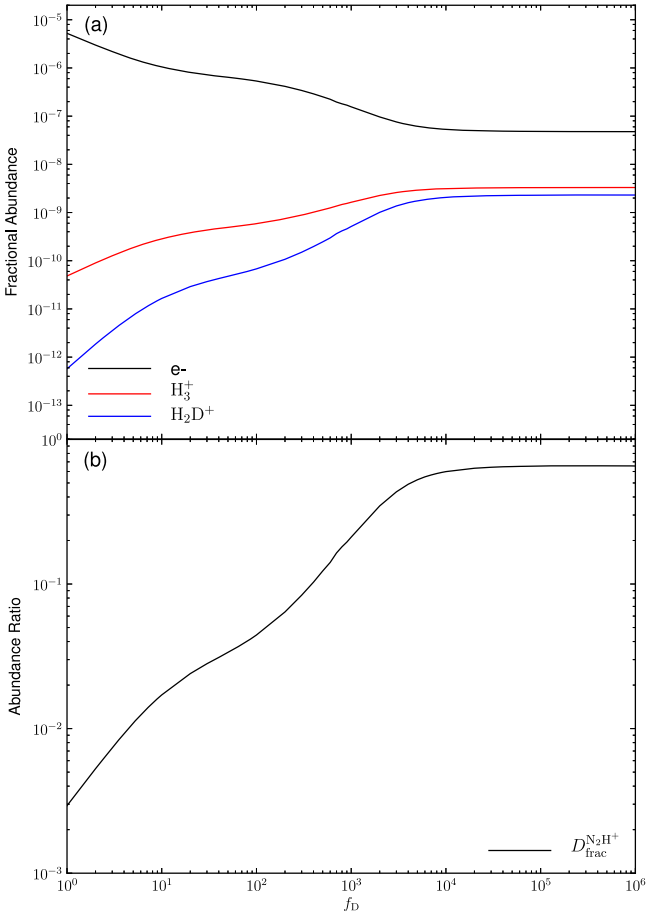


**Figure 9.** Same as Figure 8, but now all dissociative recombination reactions between electron and O-bearing species (containing no nitrogen or carbon) are removed (~40 reactions). This is used to prove that the "bump" in panel (b) of Figure 8 is caused by these reactions (no "bump" after removing the reactions). See Section 3.4.4.

### 3.6. Effect of Dynamical Density Evolution

So far we have presented models that treat density as an unchanging, controllable parameter. Here we carry out a set of dynamical density evolution (DDE) models that examine various rates of collapse relative to the free-fall rate by which a core of current density $n_{\rm H,1}$ at current time $t_1$ is created from a core at starting density $n_{\rm H,0}$ at starting time $t_0$. We parameterize the rate of density increase via

$$\frac{dn_{\rm H}}{dt} = \alpha_{\rm ff}\frac{n_{\rm H}(t)}{t_{\rm ff}(t)}, \quad (12)$$

where $t_{\rm ff}$ is the local free-fall time at the current density $n_{\rm H}$ (Equation (8)) and $\alpha_{\rm ff}$ is a parameter controlling how fast the core collapses. We define a past time variable that increases going back into a core's history via

$$t_{\rm past} = t_1 - t. \quad (13)$$

So the past density evolution is described by

$$n_{\rm H,past} = n_{\rm H,1}\left[1 + 3.60\alpha_{\rm ff}\left(\frac{n_{\rm H,1}}{10^5\ {\rm cm^{-3}}}\right)^{1/2}\left(\frac{t_{\rm past}}{10^6\ {\rm yr}}\right)\right]^{-2}. \quad (14)$$

For a given current "target" density, $n_{\rm H,1}$, we then explore different ratios of starting density: $n_{\rm H,0}/n_{\rm H,1} = 0.1$, 0.01 and three different values of $\alpha_{\rm ff} = 0.01$, 0.1, 1. We run these models for three different target densities $n_{\rm H,1} = 10^4$, $10^5$, $10^6$ cm$^{-3}$. We first start by keeping other aspects of the modeling the same as the fiducial model, i.e., a starting $\mathrm{OPR}_{\rm eq}^{\rm H_2} = 3$ and a fixed depletion factor of $f_D = 10$. The results are shown in Figure 12.

The first row of Figure 12 shows the density evolution with $t_{\rm past}$ increasing to the left. For each $n_{\rm H,1}$, the faster the collapse rate (larger $\alpha_{\rm ff}$), the shorter the past history of the core since its starting condition. Similarly, for fixed $n_{\rm H,1}$ and $\alpha_{\rm ff}$, larger values of $n_{\rm H,0}$ mean shorter core histories. The second row of Figure 12 shows the evolution of the ionization fraction, which declines as density increases. The third row shows the evolution of $\mathrm{OPR}_{\rm eq}^{\rm H_2}$, showing rapid falls from the assumed starting value of 3. Note that in some of the fast-evolving, higher density models there is insufficient time for $\mathrm{OPR}_{\rm eq}^{\rm H_2}$ to reach its equilibrium value. The fourth and fifth rows show the abundances of $N_2H^+$ and $N_2D^+$, respectively, while the bottom row shows the evolution of $D_{\rm frac}^{\rm N_2H^+}$. Again, note that in the fast-evolving, higher density models there is insufficient time to reach $D_{\rm frac,eq}^{\rm N_2H^+}$.

Note that very slowly evolving models with $t_{\rm past}$ extending beyond several $\times 10^7$ yr are unlikely to be relevant given estimated GMC lifetimes (e.g., $\sim 3 \times 10^7$ yr, Williams & McKee 1997). Considering the cases with the fastest collapse with $\alpha_{\rm ff} = 1$ that create cores with $n_{\rm H} = 10^5$–$10^6$ cm$^{-3}$ from starting conditions a factor of 10 lower in density (green solid lines in panels (i), (o), (l), (r) of Figure 12), the collapse history did not produce very low $\mathrm{OPR}^{\rm H_2}$ or very high $D_{\rm frac}^{\rm N_2H^+}$ (always $<10^{-3}$). However, models of fast collapse could potentially form highly deuterated cores if starting from lower densities (thus giving more time for chemical evolution) or, as explored below, with lower initial $\mathrm{OPR}_{\rm eq}^{\rm H_2}$ ratios.

We next re-run the above DDE models, but with time-dependent depletion/desorption starting from $f_D = 1$. These TDD+DDE models are shown in Figure 13. We find broadly similar results that rapidly collapsing high density cores have difficulty achieving high levels of $D_{\rm frac}^{\rm N_2H^+}$.

We next explore the effect of the assumed starting $\mathrm{OPR}_{\rm eq}^{\rm H_2}$ and the starting depletion factor. Focusing on models with $n_{\rm H,1} = 10^5$ and $10^6$ cm$^{-3}$ and with $\alpha_{\rm ff} = 0.01$, 0.033, 0.1, 0.33, 1, we run TDD+DDE models for initial $\mathrm{OPR}_{\rm eq}^{\rm H_2} = 0.01, 0.1, 1,$ 3 and initial $f_D = 1$, 10, 100, and show their results for $D_{\rm frac}^{\rm N_2H^+}$ in Figures 14–16.

For the models with initial $f_D = 1$, we find $D_{\rm frac}^{\rm N_2H^+} > 0.1$ cores require $\alpha_{\rm ff} \lesssim 0.33$, unless the starting $\mathrm{OPR}_{\rm eq}^{\rm H_2} = 0.01$. However, these requirements become more relaxed if we start with $f_D = 10$, 100. To reconcile models of fast collapse with high deuteration, it would require larger values of initial $f_D$ (>10) and small initial $\mathrm{OPR}_{\rm eq}^{\rm H_2}$.

In order to see if these models with different starting values of $f_D$ can be separated by absolute abundances of $[N_2H^+]$, we plot the relation between $D_{\rm frac}^{\rm N_2H^+}$ and $[N_2H^+]$ with $n_{\rm H,1} = 10^5$ cm$^{-3}$ in Figure 17 and $n_{\rm H,1} = 10^6$ cm$^{-3}$ in Figure 18. As expected, the absolute abundances are lower in models with higher initial $f_D$, so that observations of these

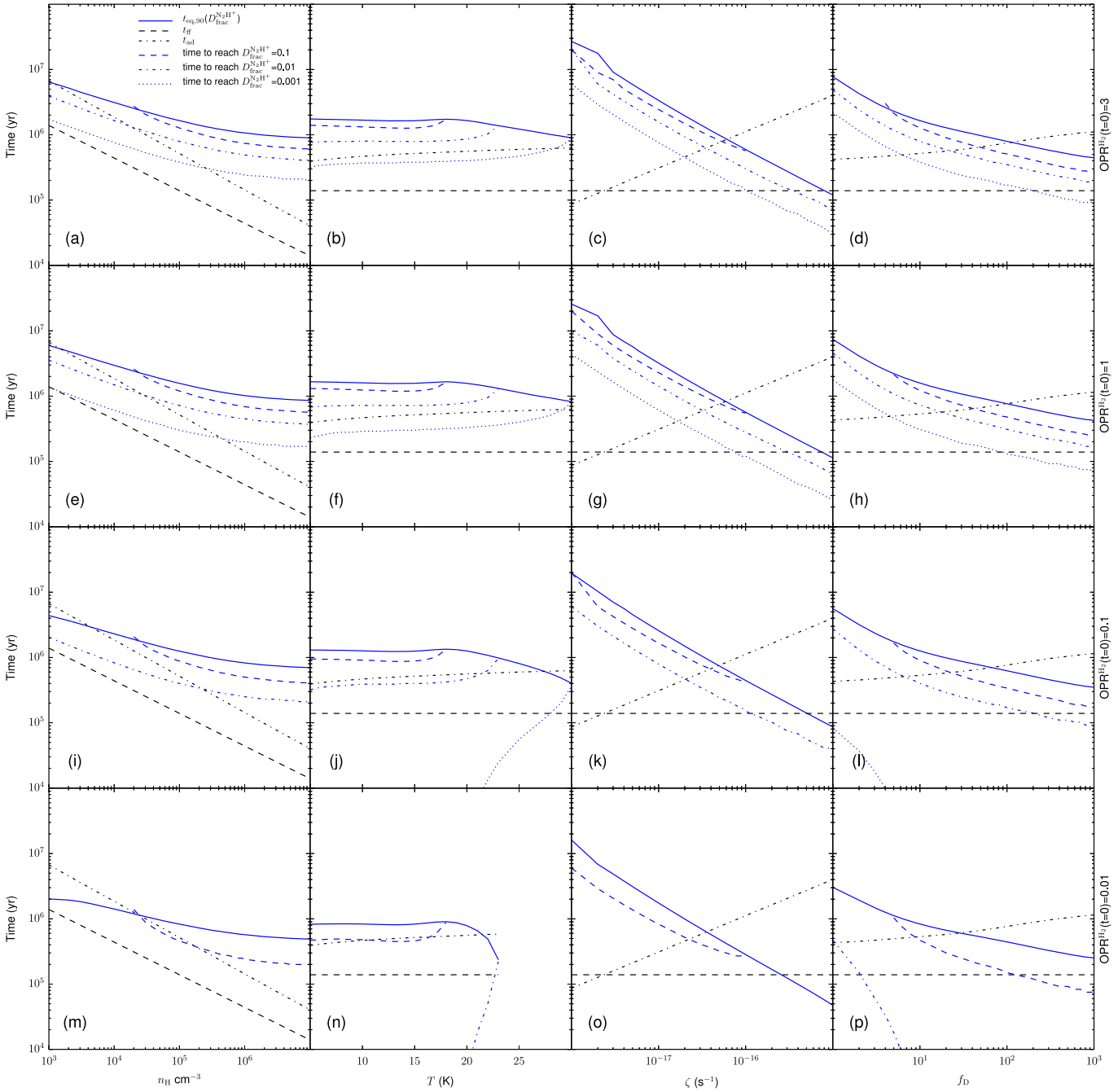


**Figure 10.** Same as bottom row of Figure 6, which now appears as the top row here. The second, third, and bottom rows show the effect of changing the initial $OPR^{H_2}$ to 1, 0.1, and 0.01, respectively. The blank parts in high-temperature exploration of the bottom row are due to this initial $OPR^{H_2} = 0.01$ being smaller than $OPR_{eq}^{H_2}$ (see panel (b) in Figure 6).

abundances, together with $D_{frac}^{N_2H^+}$, can help distinguish between the models' families.

## 4. DISCUSSION

### 4.1. Deuteration as a Chemical Clock

The high equilibrium values of $D_{frac}^{N_2H^+}$, together with the small starting fractional abundance of D relative to H and the controlling influence of the ortho-to-para ratio of $H_2$, which decays relatively slowly, mean that over a wide range of parameter space relevant for cold, dense starless cores, the timescale to reach deuteration equilibrium is relatively long compared to, for example, the local free-fall timescale. Unless the starting conditions for core formation involve extremely low values of $OPR^{H_2} \lesssim 10^{-2}$, high values of depletion factor $f_D \gtrsim 10$, or suffer high values of CR ionization $\zeta \gtrsim 10^{-16}$ s$^{-1}$, then observing high values of $D_{frac}^{N_2H^+} \gtrsim 0.1$ implies that the core is contracting at rates significantly lower than free fall, so it has been in a dense, cold state for at least several dynamical times. Note that if the core is close to chemical equilibrium, then the derived deuteration timescale is only a lower limit to its age. More accurate constraints require a tailored application

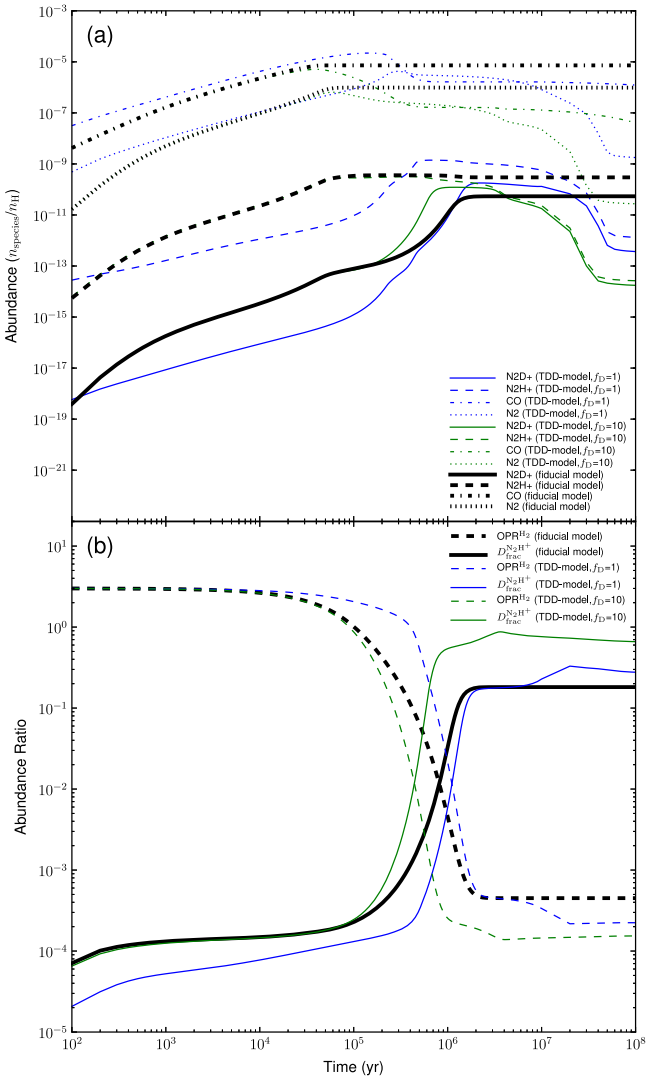


**Figure 11.** (a) Top panel: time evolution of the fractional abundances of important gas-phase species in both the fiducial model (thick black lines) and the TDD models (thin lines). The two TDD models shown here started with $f_D = 1$ (blue) and $f_D = 10$ (green). (b) Bottom panel: time evolution of gas-phase $OPR^{H_2}$ and $D_{frac}^{N_2H^+}$ in the fiducial model (thick black lines) and the TDD model (thin lines). The two TDD models shown here started with $f_D = 1$ (blue) and $f_D = 10$ (green).

of chemical models to particular physical conditions of individual cores and may require the measurement of absolute abundances to constrain the effects of the depletion factor.

In one of the best studied low-mass pre-stellar cores, L1544 in the Taurus molecular cloud, we can attempt to constrain an age. Within the central 3600 AU (the beam size of the IRAM 30 m antenna at the frequency of the $N_2H^+(1–0)$ line), $D_{frac}^{N_2H^+} = 0.2$[10] (Crapsi et al. 2005), the average number density is $n_H \simeq 10^6$ cm$^{-3}$ (Keto & Caselli 2010), the temperature is about 6 K (Crapsi et al. 2007), the CR ionization rate is $\simeq 1 \times 10^{-17}$ s$^{-1}$ and the CO depletion factor is 100 (Keto & Caselli 2010). With these parameters, we obtain the time to reach $D_{frac}^{N_2H^+} = 0.2$ to be $4.2 \times 10^5$–$2.6 \times 10^5$ yr, starting with $OPR^{H_2} = 3$–0.1, respectively, i.e., between 9.6 and 5.9 times the current value of $t_{ff}$. The corresponding value of $OPR^{H_2}$ is expected to be $\sim 3 \times 10^{-3}$.

In cases where such a detailed analysis cannot be carried out, we can still derive some limits on the core deuteration timescale. For example, $D_{frac}^{N_2H^+} \gtrsim 0.1$ has been measured in low-mass pre-stellar cores (Crapsi et al. 2005; P09) and high-mass starless cores (Fontani et al. 2011; Miettinen et al. 2012), and there are currently no values of $D_{frac}^{N_2H^+}$ observed to be greater than 1. Starting from this, we examine all our simple models used in our parameter space exploration (Section 3.4) to find how long it takes for $D_{frac}^{N_2H^+}$ to reach 0.1. The results are shown as the blue dashed lines in the 4th row of Figure 6. The "missing" parts indicate conditions under which $D_{frac}^{N_2H^+}$ fails to reach 0.1. As one can see from the figure, to reach $D_{frac}^{N_2H^+} > 0.1$, the cores should be dense ($n_H \gtrsim 5 \times 10^4$ cm$^{-3}$), cold ($T \lesssim 17$ K), at least moderately depleted ($f_D \gtrsim 6$), and with moderate CR ionization rates ($\zeta \lesssim 6 \times 10^{-17}$ s$^{-1}$). In all cases, the time to reach $D_{frac}^{N_2H^+} = 0.1$ is longer than $t_{ff}$. With moderate depletion ($f_D \lesssim 100$), the large $D_{frac}^{N_2H^+}$ ($\gtrsim$0.1) is likely to indicate a large deuteration age ($\gtrsim$ several $t_{ff}$) for the observed starless cores. As shown in Figure 10, these constraints can be somewhat relaxed if the starting $OPR^{H_2}$ values are small ($\lesssim$0.1) and the starting depletion factors are large ($f_D \gtrsim 100$) (see also discussion in Pagani et al. 2011, and Section 4.3, below).

### 4.2. Implications for Magnetic Support and Comparison with the Ambipolar Diffusion Time

If the contraction of starless cores is very slow compared to the local free-fall time, then this implies some form of pressure support is resisting collapse (see also Keto & Caselli 2010). In cores that are more massive than the thermal Bonnor–Ebert mass, such as L1544 and the massive cores studied by Tan et al. (2013), this pressure support would need to be nonthermal, i.e., turbulence or magnetic fields. However, turbulence is expected to decay relatively quickly, within $\sim 1 t_{ff}$ (Mac Low et al. 1998; Stone et al. 1998), leaving magnetic fields as the favored option. This would imply core collapse occurs on the ambipolar diffusion timescale $t_{ad}$: the timescale for neutrals in dense cores with low ionization fractions to contract relative to the magnetic field (e.g., Tassis & Mouschovias 2004).

The ambipolar diffusion timescale can be calculated using the expression $t_{ad} = 2.5 \times 10^{13} x(e)$ yr (Spitzer 1978; Shu et al. 1987), where $x(e)$ is the electron abundance relative to $n_H$. Figure 6 plots $t_{ad}$, to compare with $t_{eq,90}(D_{frac}^{N_2H^+})$ and $t_{ff}$. As $t_{ad}$ is closely related to the ionization structure in core, high density, and low $\zeta$ conditions reduce $t_{ad}$, as shown in panels (e), (g), (m), and (o). For fiducial conditions, the deuteration timescale is more similar to the local ambipolar diffusion timescale than to the free-fall time. Appreciating the caveats of estimates of deuteration timescales, discussed above, we conclude this is tentative, indirect evidence that magnetic fields are playing an important role in regulating starless core formation, and thus star formation.

[10] We note that this observed $D_{frac}^{N_2H^+}$ value should be treated as a lower limit, as this is an average along the line of sight and it is well known that the $N_2H^+(1–0)$ emission is more extended than the $N_2D^+(2–1)$ emission (Caselli et al. 2002). Therefore, our estimates of the time scales are also lower limits.

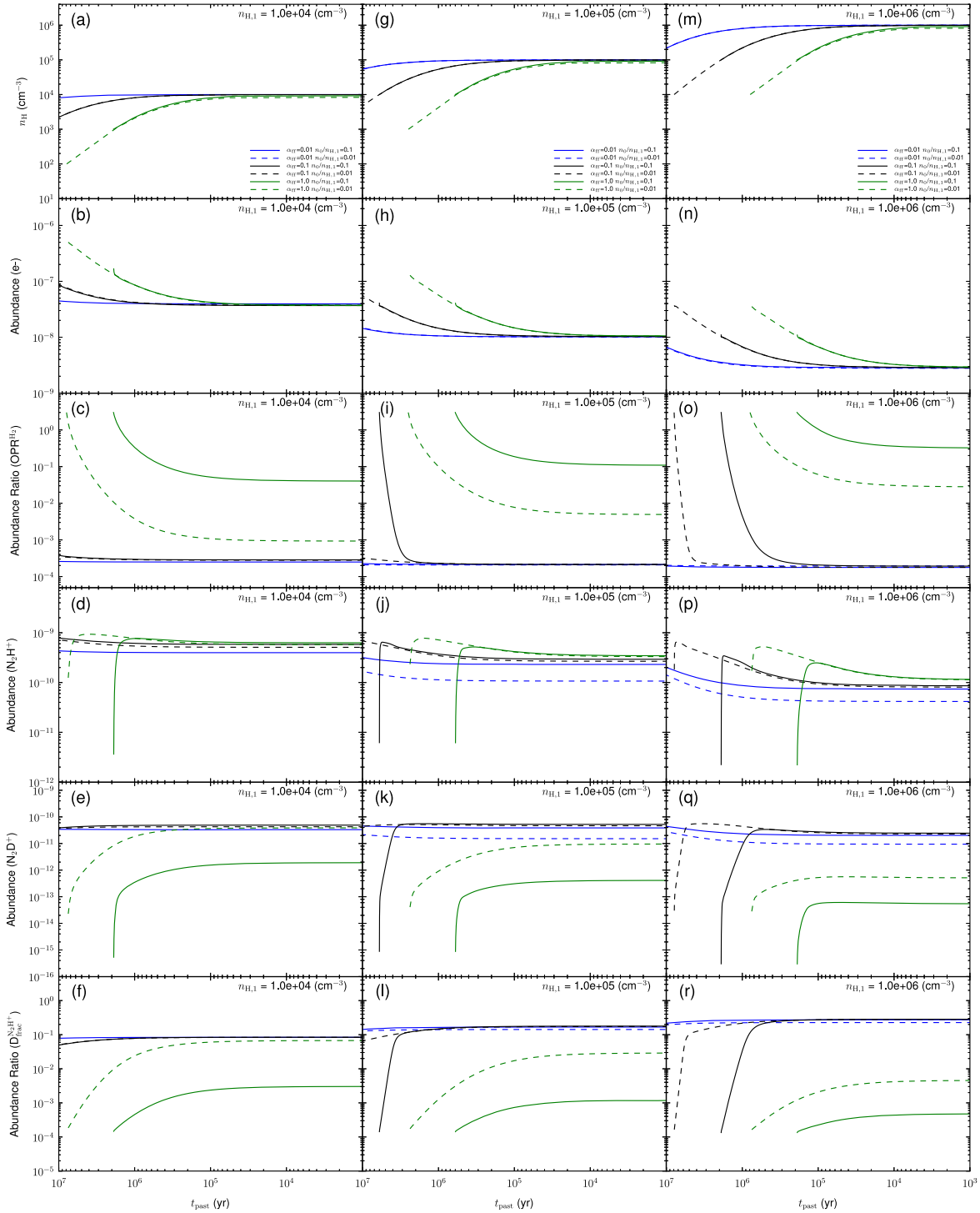


**Figure 12.** Dynamical density evolution (DDE) models that have a time-evolving density at various rates relative to free-fall collapse, as parameterized by $\alpha_{\rm ff}$ (see Equation (14)). Each column shows the results of particular target densities $n_{\rm H,1} = 10^4$, $10^5$, and $10^6$ cm$^{-3}$ (left to right). The top row shows the time evolution of the density as a function of $t_{\rm past}$, increasing to the left. In each case, models with $\alpha_{\rm ff} = 0.01$, 0.1, 1 and starting to final density ratios of $n_{\rm H,0}/n_{\rm H,1} = 0.1$, 0.01, are shown. Rows 2–6 show the time evolution of [e-], OPR$^{\rm H_2}$, [$N_2H^+$], and [$N_2D^+$], $D_{\rm frac}^{\rm N_2H^+}$, respectively.

### 4.3. Comparison to Previous Studies

There have been a number of discussions regarding the deuteration chemistry in pre-stellar cores (e.g., Pagani et al. 1992; Flower et al. 2006; P09; Sipilä et al. 2010; Parise et al. 2011; Wirström et al. 2012; Pagani et al. 2013). Compared with most of these previous studies, we have focused on $D_{\rm frac,eq}^{\rm N_2H^+}$ using a more complete cold core chemistry network and with a larger and more systematic exploration of the parameter space of environmental conditions that help control the chemistry.

In the following, we compare our model with some of these works. Parise et al. (2011) benchmarked their results against

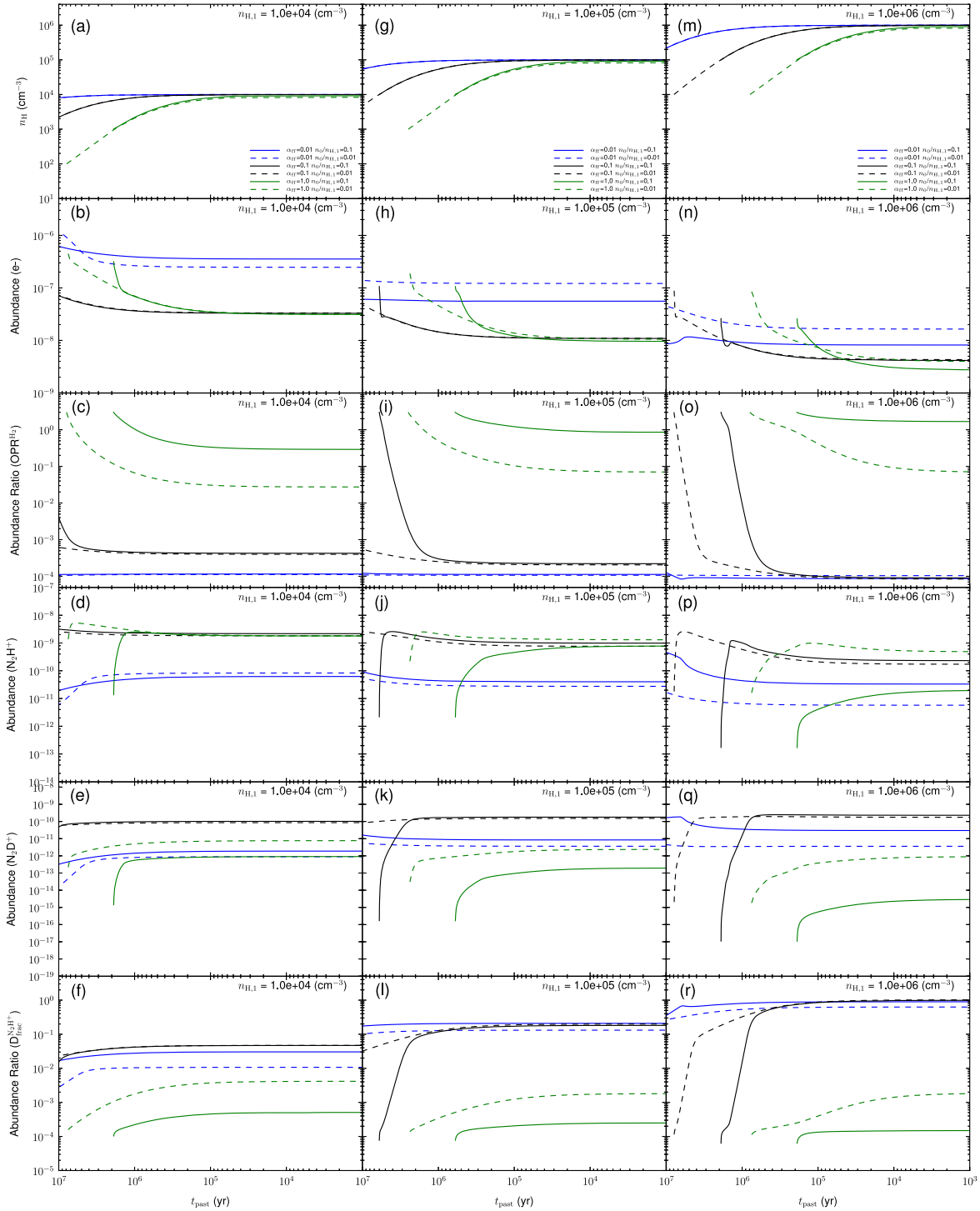


**Figure 13.** Same as Figure 12, but all models are now with Time-Dependent Depletion/Desorption (TDD).

those of P09 and Sipilä et al. (2010), but they do not show results for $D_{\rm frac}^{\rm N_2H^+}$. Both P09 and Sipilä et al. (2010) used the $H_3^+ + H_2$ reaction system of Hugo et al. (2009) (including spin states and deuterium). Sipilä et al. (2010) also used dissociative recombination reactions from P09, but no elements heavier than He were considered. Taking this into consideration, we will only compare our models directly with P09 out of these three papers. We will also compare with Wirström et al. (2012). Note that although Aikawa et al. (2012) built a comprehensive chemical/dynamical model that included deuterium chemistry and followed the evolution of pre-stellar cores to the formation of protostars, since they do not include spin state chemistry, a direct comparison with our results cannot be made.

Our work can be compared most closely to that of P09, who included spin state chemistry and modeled the evolution of the abundance ratio of $N_2D^+$ relative to $N_2H^+$ and discussed its use as a chemical clock. They used a modified version of the

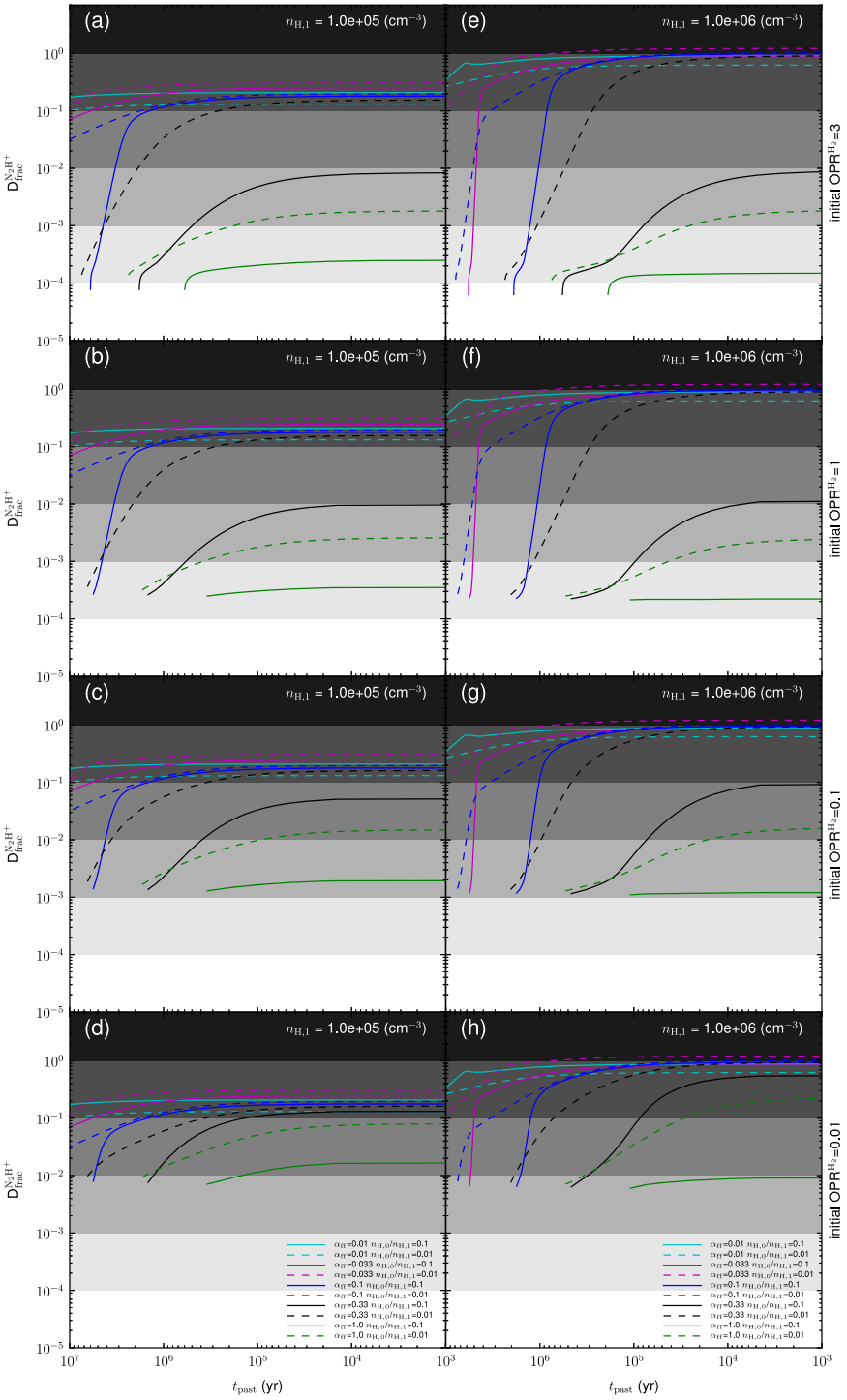


**Figure 14.** Effect of starting OPR$^{H_2}$ on $D_{frac}^{N_2H^+}$ in dynamical density evolution with time-dependent depletion/desorption (DDE+TDD) models of dense cores. Left and right columns show the results of target densities $n_{H,1} = 10^5$, and $10^6$ cm$^{-3}$, respectively. From top to bottom, the rows show a starting OPR$^{H_2}$ = 3, 1, 0.1, and 0.01, respectively. In each case, models with $\alpha_{ff}$ = 0.01, 0.033, 0.1, 0.33, 1 and starting to final density ratios of $n_{H,0}/n_{H,1}$ = 0.1, 0.01 are shown. Here the starting $f_D$ = 1.

Nahoon code to model about 35 species and 400 reactions. They did not model N chemistry: in particular the abundance of $N_2$ was a parameter in their modeling, so absolute abundances are not predicted. They developed a simple layered model for core structure that they compared to observations of the pre-stellar core L183. Based on the observed relatively low $D_{frac}^{N_2H^+}$ in the center of the core, they concluded this central region must have only attained high density relatively recently. They estimated a minimum age of $\sim 2 \times 10^5$ yr, but suggested that it may not be that much older than this.

We ran our models with P09's choices of parameters, and compared with their Figures 7–9. In particular, they used $T = 7$ K, $\zeta = 2 \times 10^{-17}$ s$^{-1}$. Their dust-to-gas mass ratio, grain radius, and dust grain density are the same as our fiducial

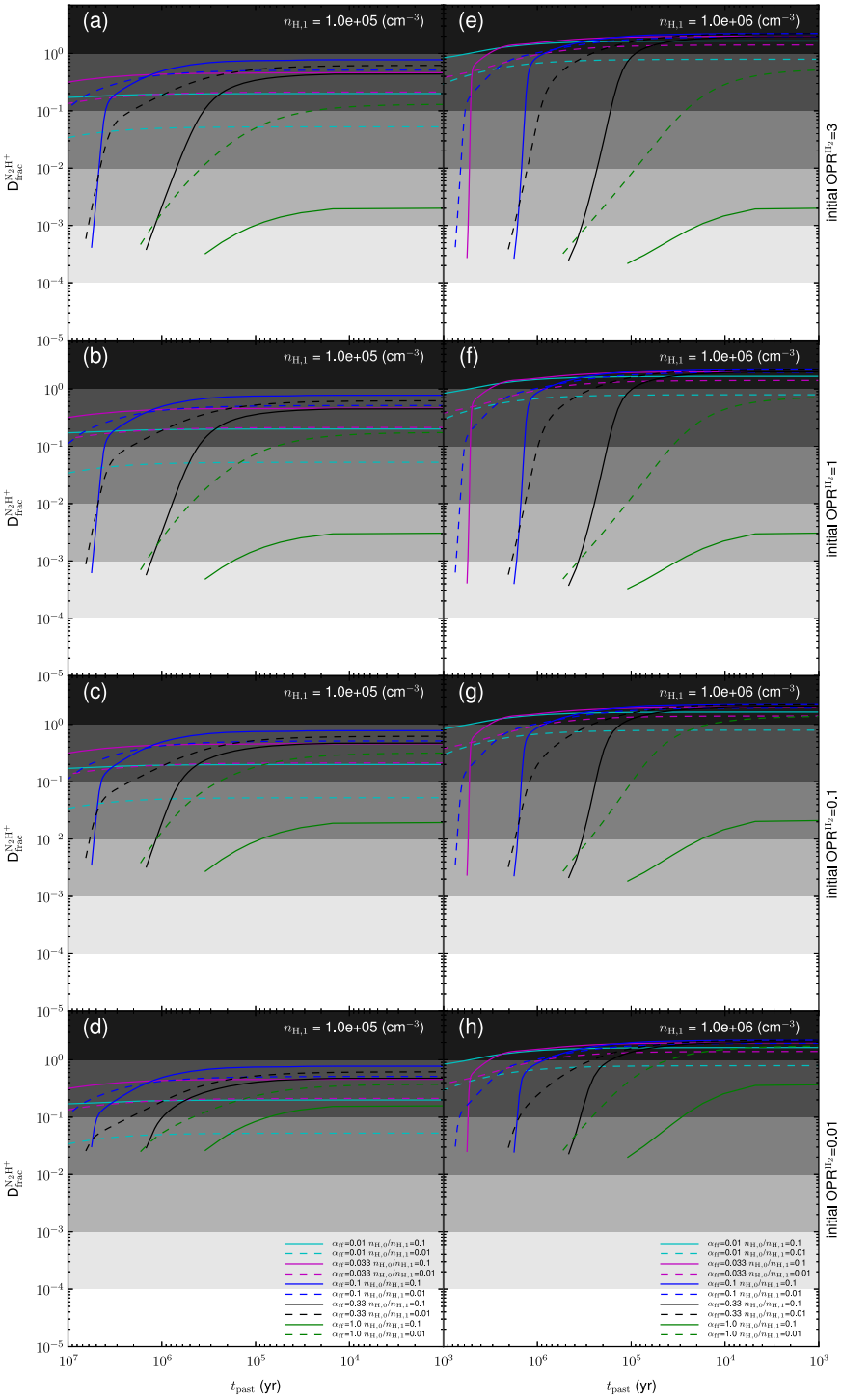


**Figure 15.** Same as Figure 14, but starting with $f_D = 10$.

model. They also used a fixed density and did not include time-dependent depletion/desorption. They set CO abundance to be $10^{-5}$ and $n_H = 1.4 \times 10^5\,cm^{-3}$ in the outer layer, and set CO abundance to be $10^{-6}$ and $n_H = 4.2 \times 10^6\,cm^{-3}$ in the inner layer. It is unclear whether they had leftover C and O atoms in their models. Here we simply assume all C and O were in CO in their models. Moreover, it is not clear what initial $[N_2]$ they used in the models (this was an input parameter of their models). We try our fiducial [N] in both runs (case 1). We also tried two more models with the $[N_2] = [CO]$ value of P09 (case 2). We utilize P09's starting value of $OPR^{H_2} = 3$.

The results of our models are summarized in Table 4 and compared with P09. We first look at the timescales. For the outer shell, the four timescales reported by our model are generally ~2–3 times that of P09 models. But for the inner shell our results are closer to those of P09. Recalling our parameter space exploration in Figure 6, the depletion factor $f_D$ has a strong effect on the equilibrium timescales. Since it is

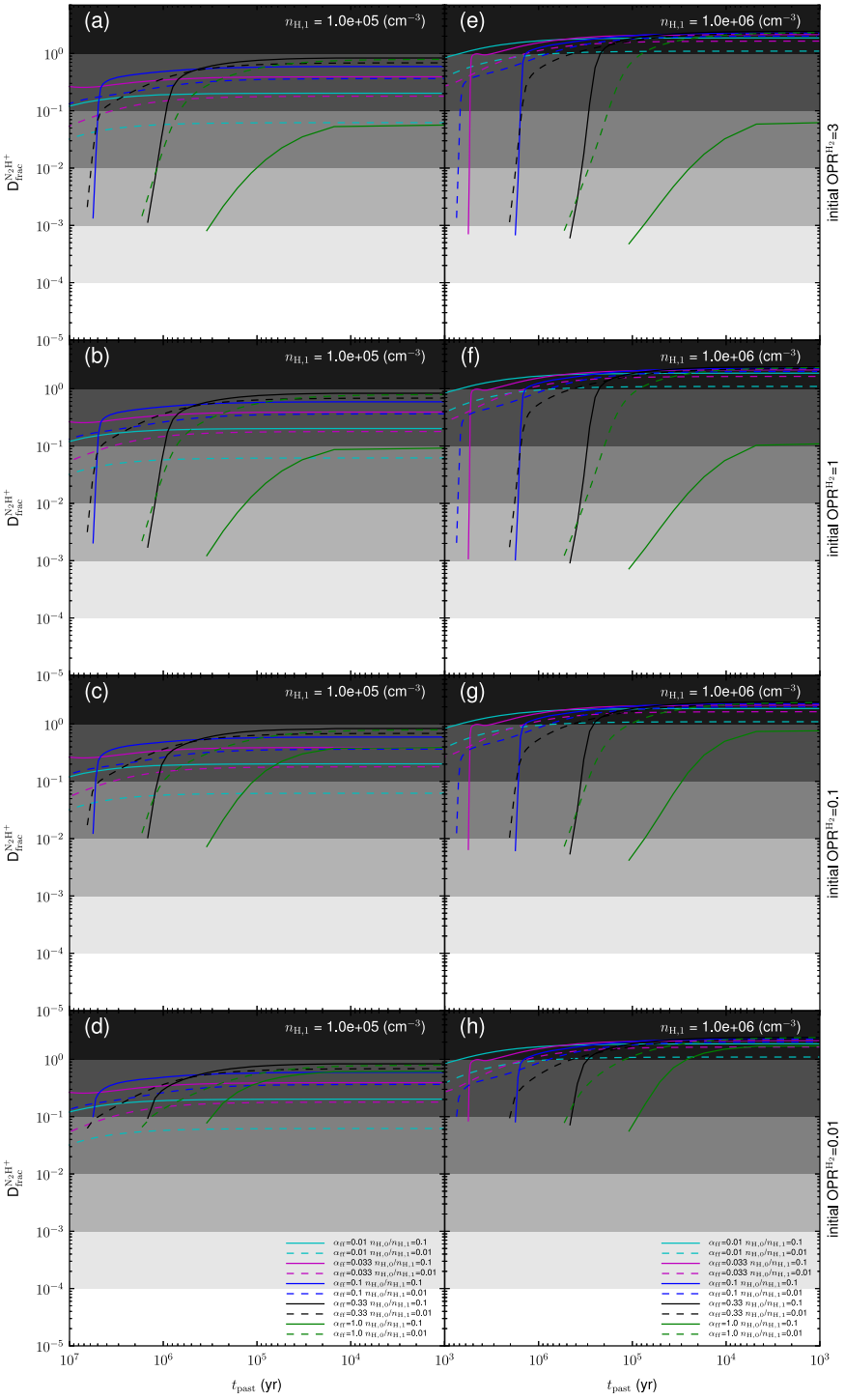


**Figure 16.** Same as Figure 14, but starting with $f_D = 100$.

unclear what were the exact abundances used by P09 for C, N, and O, the difference of the timescales in Table 4 could be due to differences in abundances, i.e., depletion factor.

The fact that our fiducial model is somewhat slower compared to P09's Figure 7 is likely due to their choice of stronger depletion. Recalling our Figure 6, the high density in the P09 cores shortens the equilibrium timescale somewhat, but this is compensated by P09's choice of a slightly smaller $\zeta$. However, the large depletion factor can greatly shorten the equilibrium time. In P09's inner shell $[CO] = 10^{-6}$ (if they did not have leftover atomic C and O), then this corresponds to $f_D = 146$ for C and $f_D = 360$ for O based on our choices for initial elemental abundances, which would greatly shorten the timescales if $f_D$ for N is comparable to our models.

In P09's Figure 7, the equilibrium time for $D_{frac}^{N_2H^+}$ was ~5 times longer than the local instantaneous free-fall time. However, their conclusion was that the core did not reach the equilibrium. Our model predicts a much longer chemical

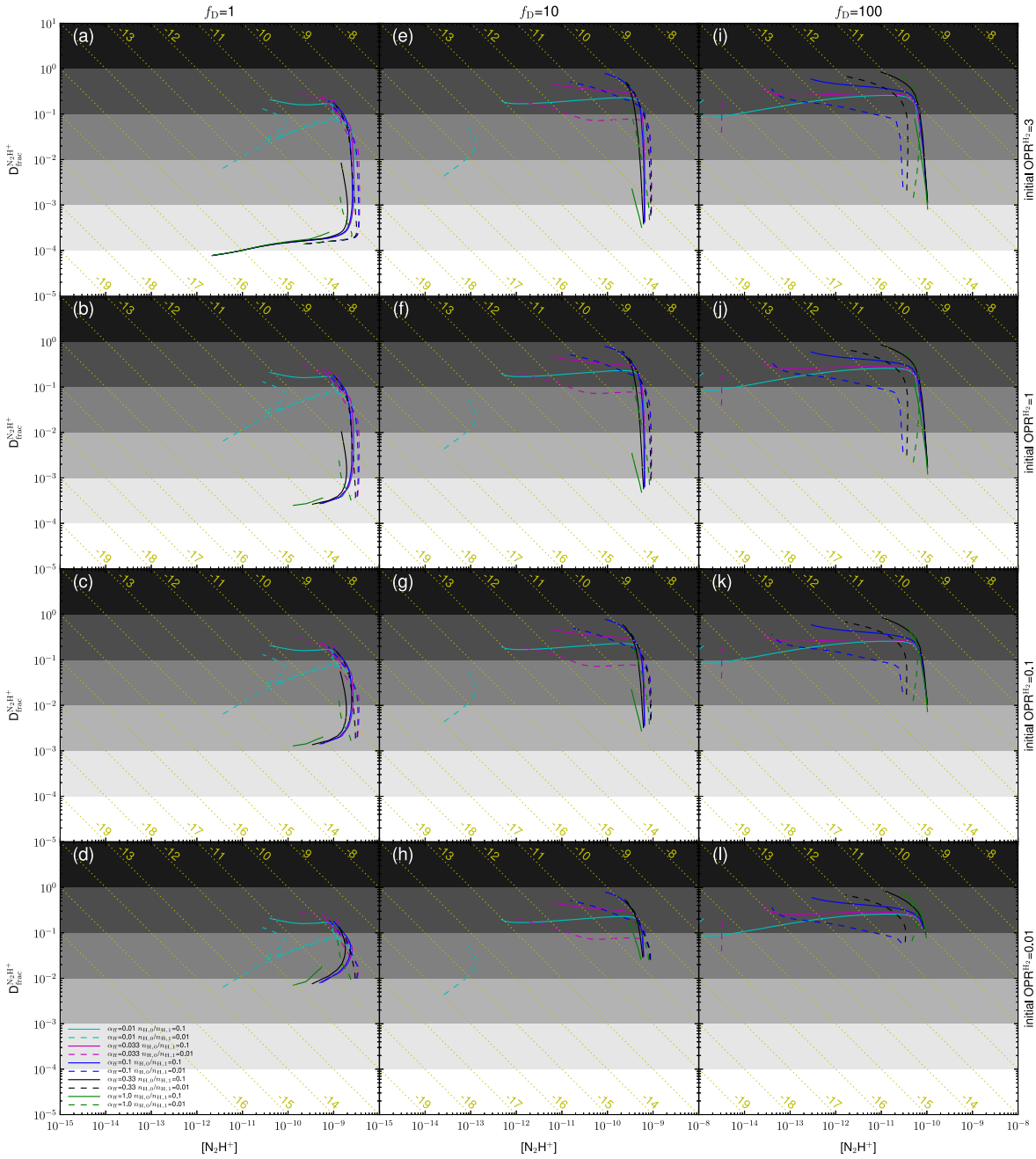


**Figure 17.** Relation between $D_{\rm frac}^{\rm N_2H^+}$ and [$N_2H^+$], with different starting $f_D$ (labeled on top) and OPR$^{H_2}$ (labeled on right). The modeled cores in this figure are from those in Figures 14–16, having $n_{\rm H,1} = 10^5$ cm$^{-3}$. The yellow dotted lines show constant [$N_2D^+$] (the yellow numbers are indices with the base of 10).

equilibrium timescale compared to the local free-fall time (also dependent on $f_D$). If we were to observe cores with the relevant high $D_{\rm frac}^{\rm N_2H^+}$, then their ages should be relatively old.

Therefore, in terms of $D_{\rm frac,eq}^{\rm N_2H^+}$ and $t_{\rm eq,90}(D_{\rm frac}^{\rm N_2H^+})$, our model agrees with P09 within a factor of 2–3. The major differences come from the assumption of initial depletion and core equilibrium state. These need to be constrained by observations.

Wirström et al. (2012) used a network with 4420 reactions, and their equilibrium time for OPR$^{H_2}$ is larger than $10^6$ yr, which is more similar to our value. They used $n_{\rm H} = 2 \times 10^6$ cm$^{-3}$, $T = 10$ K, $A_V > 10$ mag, and $\zeta = 3 \times 10^{-17}$ s$^{-1}$, starting with OPR$^{H_2} = 3$. They allowed all neutral species (except for $H_2$, He, N, and $N_2$) to freeze-out, but no desorption was considered. One thing to note is that we are not sure about what initial elemental abundances Wirström et al. (2012) used. They reference Savage & Sembach (1996), who reported elemental abundances in a variety of environments. We are not sure what specific initial abundances Wirström et al. (2012) used. So the comparison here is just qualitative.

## 5. CONCLUSIONS

We have presented a parameter space exploration of the deuterium fractionation process, in particular of $N_2H^+$, in conditions appropriate to starless dense cloud cores in

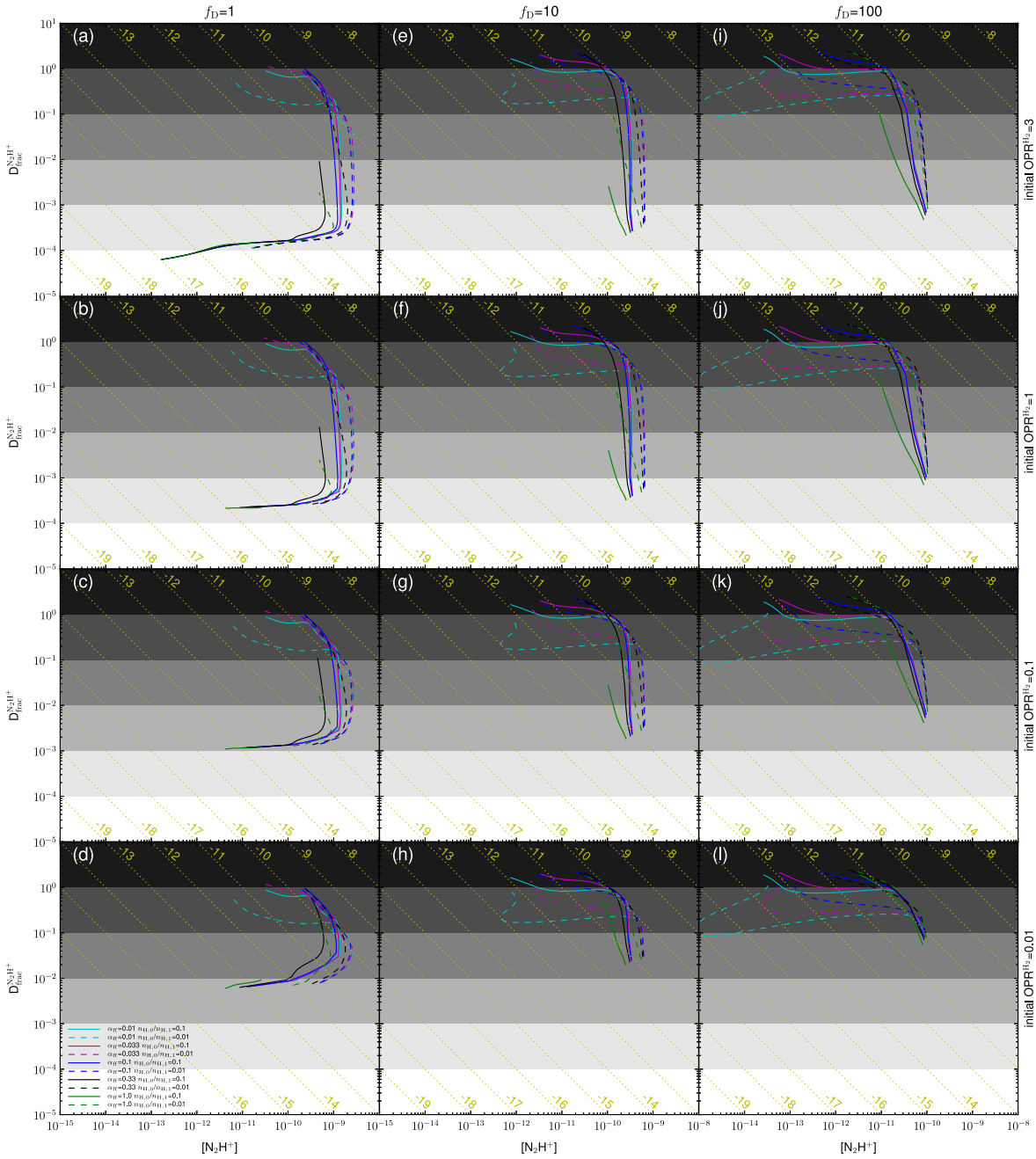


**Figure 18.** Same as Figure 17, but with $n_{H,1} = 10^6$ cm$^{-3}$.

different environments. An enhanced 3-atom reaction network is introduced. It was derived from a reduced chemical network extracted from the KIDA database to which deuterium and spin state chemistry has been included. Reactions involving $H_3O^+$ and its deuterated forms are introduced from Sipilä et al. (2013), to be able to reproduce results from the more comprehensive model of Sipilä et al. (2013). The effects of time-dependent depletion and dynamical density evolution have also been examined. Compared to previous studies (e.g., Pagani et al. 2009), our focus is on conditions that are also relevant for massive star formation, such as the massive starless cores observed by Tan et al. (2013). Our main results are as follows:

1. Based on our fiducial modeling, the equilibrium value of $[N_2D^+]/[N_2H^+]$ monotonically increases with increasing density (from $10^3$ cm$^{-3} < n_H < 10^7$ cm$^{-3}$), and decreasing CR ionization rate ($10^{-18}$ s$^{-1} < \zeta < 10^{-15}$ s$^{-1}$). With increasing temperature, the equilibrium $[N_2D^+]/[N_2H^+]$ first moderately increases from $T \simeq 5$ K to $T \simeq 13$ K, then decreases to $T \simeq 30$ K. With increasing freeze-out, the equilibrium $[N_2D^+]/[N_2H^+]$ increases from $f_D \simeq 1$ to $f_D \simeq 1000$, but drops from $f_D \simeq 2000$ to $f_D \simeq 10^6$.
2. When the gas temperature exceeds $\simeq$20 K, the ortho-to-para $H_2$ ratio increases, reducing the deuterium fraction so that warmer starless cores should display lower deuterium fractions (as found in high-mass star-forming regions by Fontani et al. 2011).

**Table 4**
Comparison with P09 Models of Inner and Outer Shells

| Model | $OPR_{eq}^{H_2}$ ($\times 10^{-4}$) | $t_{eq}(OPR^{H_2})$ ($10^6$ yr) | $t_{eq,90}(OPR^{H_2})$ ($10^6$ yr) | $D_{frac,eq}^{N_2H^+}$ | $t_{eq}(D_{frac}^{N_2H^+})$ ($10^6$ yr) | $t_{eq,90}(D_{frac}^{N_2H^+})$ ($10^6$ yr) |
|---|---|---|---|---|---|---|
| Outer shell (P09)[a] | 0.99 | 0.80 | 0.69 | 0.71 | 0.84 | 0.54 |
| Outer shell (case1)[b] | 1.15 | 1.90 | 1.28 | 0.399 | 1.64 | 1.02 |
| Outer shell (case2)[c] | 1.41 | 2.30 | 1.57 | 0.289 | 1.98 | 1.25 |
| Inner shell (P09)[a] | 0.53 | 0.38 | 0.28 | 5.9 | 0.30 | 0.17 |
| Inner shell (case1)[b] | 0.326 | 0.575 | 0.340 | 2.24 | 0.465 | 0.234 |
| Inner shell (case2)[c] | 0.299 | 0.515 | 0.298 | 2.96 | 0.415 | 0.200 |

**Notes.**
[a] The P09 values are read from their figures using the Dexter tool incorporated in A&A online journal, for which we estimate ~1% uncertainties.
[b] In this case we used [N] in our fiducial model.
[c] In this case we used [N] = [CO] in P09.

3. The above findings are robust against changes in the initial elemental and molecular abundances.
4. Constraints on core ages and collapse rates can be obtained if accurate measurements of $[N_2D^+]/[N_2H^+]$ are made, coupled with observations of core density, temperature, and (CO) depletion structure. However, results can also depend on the CR ionization rate and the initial ortho-to-para ratio of $H_2$.
5. In the case of the well-known low-mass pre-stellar core L1544, we estimate that the gas within the central 3600 AU has a deuteration age between $\simeq$6 and 10 times the current local free-fall time, depending on the initial value of the ortho-to-para $H_2$ ratio.
6. More generally, to reproduce the typical deuterium fractions measured toward low-mass and massive pre-stellar cores ($[N_2D^+]/[N_2H^+] \gtrsim 0.1$), the following physical parameters are needed: $n_H \gtrsim 3 \times 10^4$ cm$^{-3}$, $T \lesssim 17$ K, depletion factor $\gtrsim$6, and CR ionization rate $\lesssim 10^{-16}$ s$^{-1}$. In general, these values of deuterium fractions require timescales several times longer than the local free-fall timescale. With no initial depletion, the inclusion of time-dependent depletion/desorption has only a modest effect on these conclusions. Also, with no initial depletion, models with dynamically evolving density, increasing by a factor of 10, require collapse rates about 10 times slower than free-fall to reach the above levels of deuteration in cores with $n_H = 10^6$ cm$^{-3}$. This suggests that dense cores with large deuterium fractions are dynamically old, which would likely require support against gravity to be provided by magnetic fields. For our fiducial model parameters, the timescale to reach deuteration equilibrium is similar to the expected ambipolar diffusion timescale, i.e., the collapse time of a magnetically subcritical core. The above conclusions can be avoided if the initial depletion factor is $\gtrsim$10 (in which case rapidly collapsing cores could reach $[N_2D^+]/[N_2H^+] \gtrsim 0.1$), the CR ionization rate is very high ($\gtrsim 10^{-16}$ s$^{-1}$) or if the initial ortho-to-para ratio of $H_2$ in the core is very small ($\lesssim$0.01), although this last condition itself would require the parental cloud to have a significant age.

The authors acknowledge the continuous and fruitful interactions with Jorma Harju, and an anonymous referee for helping improve the manuscript. S.K. acknowledges support from Xueying Tang and an NRAO Student Observing Support grant. J.C.T. acknowledges support from the University of Florida Research Opportunity Seed Fund and the Florida Space Inst. V.W. acknowldeges funding by the French INSU/CNRS program PCMI, the Observatoire Aquitain des Sciences de l'Univers and the European Research Council (ERC Grant 336474: 3DICE).

## REFERENCES

Aikawa, Y., Wakelam, V., Hersant, F., Garrod, R. T., & Herbst, E. 2012, ApJ, 760, 40
Bacmann, A., Lefloch, B., Ceccarelli, C., et al. 2003, ApJL, 585, L55
Bergin, E. A., Plume, R., Williams, J. P., & Myers, P. C. 1999, ApJ, 512, 724
Bergin, E. A., & Tafalla, M. 2007, ARA&A, 45, 339
Bisschop, S. E., Fraser, H. J., Öberg, K. I., van Dishoeck, E. F., & Schlemmer, S. 2006, A&A, 449, 1297
Bodenheimer, P. H. 2011, Principles of Star Formation (Berlin: Springer)
Brünken, S., Sipilä, O., Chambers, E. T., et al. 2014, Natur, 516, 219
Butler, M. J., & Tan, J. C. 2012, ApJ, 754, 5
Caselli, P. 2002, P&SS, 50, 1133
Caselli, P., Vastel, C., Ceccarelli, C., et al. 2008, A&A, 492, 703
Caselli, P., Walmsley, C. M., Tafalla, M., Dore, L., & Myers, P. C. 1999, ApJL, 523, L165
Caselli, P., Walmsley, C. M., Terzieva, R., & Herbst, E. 1998, ApJ, 499, 234
Caselli, P., Walmsley, C. M., Zucconi, A., et al. 2002, ApJ, 565, 344
Ceccarelli, C., Hily-Blant, P., Montmerle, T., et al. 2011, ApJL, 740, L4
Crabtree, K. N., Indriolo, N., Kreckel, H., Tom, B. A., & McCall, B. J. 2011, ApJ, 729, 15
Crapsi, A., Caselli, P., Walmsley, C. M., et al. 2005, ApJ, 619, 379
Crapsi, A., Caselli, P., Walmsley, M. C., & Tafalla, M. 2007, A&A, 470, 221
Dalgarno, A. 2006, PNAS, 103, 12269
Dalgarno, A., & Lepp, S. 1984, ApJL, 287, L47
Draine, B. T., & Sutin, B. 1987, ApJ, 320, 803
Draine, B. T. 2011, Physics of the Interstellar and Intergalactic Medium by Bruce T Draine (Princeton, NJ: Princeton Univ. Press)
Emprechtinger, M., Caselli, P., Volgenau, N. H., Stutzki, J., & Wiedner, M. C. 2009, A&A, 493, 89
Flower, D. R., Pineau Des Forêts, G., & Walmsley, C. M. 2006, A&A, 449, 621
Fontani, F., Caselli, P., Crapsi, A., et al. 2006, A&A, 460, 709
Fontani, F., Palau, A., Caselli, P., et al. 2011, A&A, 529, L7
Fontani, F., Zhang, Q., Caselli, P., & Bourke, T. L. 2009, A&A, 499, 233
Friesen, R. K., di Francesco, J., Myers, P. C., et al. 2010, ApJ, 718, 666
Garrod, R. T., Wakelam, V., & Herbst, E. 2007, A&A, 467, 1103
Guelin, M., Langer, W. D., Snell, R. L., & Wootten, H. A. 1977, ApJL, 217, L165

Hasegawa, T. I., & Herbst, E. 1993, MNRAS, 261, 83
Hasegawa, T. I., Herbst, E., & Leung, C. M. 1992, ApJS, 82, 167
Hernandez, A. K., Tan, J. C., Caselli, P., et al. 2011, ApJ, 738, 11
Hily-Blant, P., Walmsley, M., Pineau Des Forêts, G., & Flower, D. 2010, A&A, 513, A41
Hugo, E., Asvany, O., & Schlemmer, S. 2009, JChPh, 130, 164302
Keto, E., & Caselli, P. 2010, MNRAS, 402, 1625
Le Petit, F., Roueff, E., & Le Bourlot, J. 2002, A&A, 390, 369
Lesaffre, P., Belloche, A., Chièze, J.-P., & André, P. 2005, A&A, 443, 961
Li, X., Heays, A. N., Visser, R., et al. 2013, A&A, 555, A14
Mac Low, M.-M., Klessen, R. S., Burkert, A., & Smith, M. D. 1998, PhRvL, 80, 2754
Maret, S., & Bergin, E. A. 2007, ApJ, 664, 956
Miettinen, O., Harju, J., Haikala, L. K., & Juvela, M. 2012, A&A, 538, A137
Oka, T. 2004, JMoSp, 228, 635
Oliveira, C. M., Hébrard, G., Howk, J. C., et al. 2003, ApJ, 587, 235
Pagani, L., Lesaffre, P., Jorfi, M., et al. 2013, A&A, 551, A38
Pagani, L., Roueff, E., & Lesaffre, P. 2011, ApJL, 739, L35
Pagani, L., Salez, M., & Wannier, P. G. 1992, A&A, 258, 479
Pagani, L., Vastel, C., Hugo, E., et al. 2009, A&A, 494, 623
Parise, B., Belloche, A., Du, F., Güsten, R., & Menten, K. M. 2011, A&A, 526, A31
Pillai, T., Caselli, P., Kauffmann, J., et al. 2012, ApJ, 751, 135
Pillai, T., Wyrowski, F., Carey, S. J., & Menten, K. M. 2006, A&A, 450, 569
Pillai, T., Wyrowski, F., Hatchell, J., Gibb, A. G., & Thompson, M. A. 2007, A&A, 467, 207
Pineau des Forets, G., Flower, D. R., & McCarroll, R. 1991, MNRAS, 248, 173
Ragan, S. E., Bergin, E. A., & Wilner, D. 2011, ApJ, 736, 163
Savage, B., & Sembach, K. 1996, ARA&A, 34, 279
Shu, F. H., Adams, F. C., & Lizano, S. 1987, ARA&A, 25, 23
Sipilä, O., Caselli, P., & Harju, J. 2013, A&A, 554, A92
Sipilä, O., Hugo, E., Harju, J., et al. 2010, A&A, 509, A98
Spitzer, L., Jr 1978, Physical Processes in the Interstellar Medium (Princeton, NJ: Princeton Univ. Press)
Stone, J. M., Ostriker, E. C., & Gammie, C. F. 1998, ApJL, 508, L99
Tan, J. C., Beltran, M. T., Caselli, P., et al. 2014, arXiv:1402.0919
Tan, J. C., Kong, S., Butler, M. J., Caselli, P., & Fontani, F. 2013, ApJ, 779, 96
Tassis, K., & Mouschovias, T. C. 2004, ApJ, 616, 283
Troscompt, N., Faure, A., Maret, S., et al. 2009, A&A, 506, 1243
van der Tak, F. F. S., & van Dishoeck, E. F. 2000, A&A, 358, L79
Vastel, C., Caselli, P., Ceccarelli, C., et al. 2012, A&A, 547, A33
Wakelam, V., & Herbst, E. 2008, ApJ, 680, 371
Wakelam, V., Herbst, E., Loison, J.-C., et al. 2012, ApJS, 199, 21
Walmsley, C. M., Flower, D. R., & Pineau des Forêts, G. 2004, A&A, 418, 1035
Ward-Thompson, D., Motte, F., & Andre, P. 1999, MNRAS, 305, 143
Williams, J. P., & McKee, C. F. 1997, ApJ, 476, 166
Wirström, E. S., Charnley, S. B., Cordiner, M. A., & Milam, S. N. 2012, ApJL, 757, L11
Wootten, A., Snell, R., & Glassgold, A. E. 1979, ApJ, 234, 876